WADC TECHNICAL REPORT 57-356
ASTIA DOCUMENT No. AD 130779

AN EXPERIMENTAL STUDY OF AN AERODYNAMIC RECTIFIER

FREDERICK O. WOOTEN

ALL AMERICAN ENGINEERING COMPANY

JUNE 1957

AERONAUTICAL RESEARCH LABORATORY
CONTRACT NO. AF 33(616)-2969
PROJECT NO. 3084
TASK NO. 70178

WRIGHT AIR DEVELOPMENT CENTER
AIR RESEARCH AND DEVELOPMENT COMMAND
UNITED STATES AIR FORCE
WRIGHT-PATTERSON AIR FORCE BASE, OHIO

Carpenter Litho & Prtg. Co., Springfield, O.
300 — October 1957

FOREWORD

The research described in this report was accomplished by the Applied Physics Department, All American Engineering Company, Wilmington, Delaware. Dr. Frederick O.Wooten, Staff Physicist, directed the project. The work was sponsored by the Aeronautical Research Laboratory, Wright Air Development Center, Wright-Patterson Air Force Base, Ohio under Air Force Contract AF33(616)2969, Project 3084, "Fuel and Propellant Sub-System, Task 70178, and covers the period from 1 May 1955 to 17 May 1957. Mr. Maurice O. Lawson of the Fluid Dynamics Research Branch, Aeronautical Research Laboratory, acted as project scientist.

Appreciation is extended to Mr. James L. Guenver of the Applied Physics Department, All American Engineering Company, for providing instrumentation. Others who contributed in the research were: Mr. Raymond B. Janney, II, Chief Engineer, and Mr. Charles Harwell, Project Engineer, All American Engineering Company; Dr. Nicholas Rott of the Graduate School of Aeronautical Engineering, Cornell University; Dr. Ralph W. Detra and Mr. P. H. Rose of Avco Advanced Development Division.

The original idea for the aerodynamic rectifier described in this report is that of Dr. Arthur Kantrowitz, Director of Research Laboratory, Avco Advanced Development Division, Avco Manufacturing Corporation. His contribution to the work before the initiation of this contract, as well as his suggestions at various times during the research program, are gratefully acknowledged.

ABSTRACT

Design and principles of operation of an aerodynamic rectifier having no moving parts are presented. For a pressure drop of one psi, it has been possible to achieve ten times as much mass flow in one direction as the other. Steady flow test results indicate that increased performance can be obtained. Unsteady flow tests indicate that about fourteen milliseconds are required after the arrival of a pressure pulse for the rectifier to resist further passage of fluid flow. This time is longer, by a factor of about four, than the time required for the passage of a sound wave through the rectifier. Leakage during the starting interval is just equal to the mass flow through a duct having the same free flow cross-sectional area.

PUBLICATION REVIEW

This report has been reviewed and is approved.

Nathan L. Krisberg

NATHAN L. KRISBERG, Colonel, USAF
Chief, Aeronautical Research Laboratory
Directorate of Research

TABLE OF CONTENTS

LIST OF APPENDIXES

LIST OF ILLUSTRATIONS

LIST OF TABLES

LIST OF SYMBOLS

a^* nondimensional speed of sound

A cross-sectional area

A_o cross-sectional area of duct between pressure vessel and aerodynamic rectifier

C_p specific heat at constant pressure

C_v specific heat at constant volume

p^* nondimensional pressure (atmospheres)

$P = \frac{2}{\gamma - 1} a + u$

$Q = \frac{2}{\gamma - 1} a - u$

} Riemann variables

u nondimensional flow velocity relative to the duct

$\gamma = \frac{C_p}{C_v}$ ratio of specific heats

ξ fractional or nondimensional distance from discharge end of unsteady flow test stand (the total test stand length is taken as unity)

ρ^* nondimensional density

$\tau = \frac{\xi}{a}^*$ nondimensional time

L, R conditions on the left, or right, side of an area discontinuity

1,2,3,.. regions of constant state in a wave diagram

$_o$ subscript specifies standard atmosphere reference conditions

$_i$ subscript refers to initial conditions prior to puncturing diaphragm

* standard atmospheric conditions are expressed as unity

INTRODUCTION

An aerodynamic rectifier is a device which permits fluid flow in one direction but greatly restricts it in the reverse direction. A distinguishing characteristic of such a rectifier is that it has no moving parts. Consequently it should have numerous applications in fluid flow problems where it is undesirable to use a mechanical check valve. In particular, it might be useful as a valve for a pulse-jet engine. For such an application, it would have the advantage of having no structural inertia to overcome as is the case with the conventional flapper valve. It would not be subject to the problems of wear inherent in apparatus with moving parts. In addition, it would permit much more freedom in the selection of materials to withstand the high temperatures of combustion.

Earlier aerodynamic rectifiers have been designed by both Tesla and Wislicenus. Tesla's rectifier (reference 1) operates by interposing sharp edges in the restricted flow direction. The sharp edges are designed to create turbulence and large separated flow regions to restrict the flow in one direction while only surface friction retards flow in the other direction. The principle of the type due to Wislicenus (reference 2) is to create a swirl for one flow direction. After passing through the section designed to create swirl, the fluid is confined to a passage of smaller diameter. This results in a higher peripheral velocity and an attendant increase in centrifugal force which tends to restrict the flow. Thus the energy in the fluid itself is used to resist flow. In reference 5, Bertin gives a performance coefficient of about 5 for the Tesla type rectifier. That is, there is about five times the flow in the free flow direction for a given pressure drop. A performance coefficient of four is given for the centrifugal type due to Wislicenus. More recently,Linderoth (reference 4) has proposed a new design for a rectifier but apparently it has not yet been tested.

The aerodynamic rectifier described in this report (see figures 2 to 5) was suggested by Kantrowitz (reference 6). It provides for one of two stable flows, depending upon the flow direction. For flow in the free flow direction the stable flow is axial, while in the restricted flow direction the stable flow follows a helical path. A developed view of a cylindrical section of the rectifier is shown in figure 1. The blade configuration shown provides a way of achieving a helical flow path for restricted flow. The first few blades in each blade column turn the flow so that it enters the high solidity cascade section at the proper angle. The performance of the rectifier is obtained in the cascade section. As the flow exits from a cascade, it has an upstream component of momentum which works against the local pressure gradient. In the presence of the pressure gradient, the streamlines are curved downstream so that the flow enters the next cascade column as depicted. In this method, the energy in the fluid itself is used to resist the flow.

The scheme just discussed is quite idealized. The actual performance of the configuration depends upon such things as three dimensional flow effects and losses due to friction and viscosity. There are, of course, some frictional effects for axial flow when operating in the free flow direction. However, these effects are very nearly the same for small variations in the basic design. Hence, finding the geometrical configuration which yields optimum performance consists, in the main, of finding the blade profiles and blade configuration which forces the fluid to follow the idealized flow path with a minimum of loss when operating in the restricted flow direction.

Manuscript released by the author 14 June 1957 for publication as a WADC Technical Report

DESIGN OF THE AERODYNAMIC RECTIFIER

Photographs showing various views of the aerodynamic rectifier and its components are shown in figures 2 to 8. The photographs with their underlying captions, together with the following paragraphs, provide a rather complete description of the rectifier used for testing purposes.

The rectifier consists of hardwood blades attached by bolts to a hollow steel core. The core is of six inch outside diameter and has a wood nose and tail section. The rectifier is enclosed in a cylindrical plexiglass shell for flow visualization purposes. Dimensions of the shell are 11-3/4 inches inside diameter, 48 inches length, and 3/16 inch wall thickness.

The hollow steel core is made in sections of 12 inches length each. This permits variation in the rectifier length, and also facilitates changes in blade configuration or angle of attack. Each section of the core has flats machined on four sides to allow the blades to have variable angle of attack. Four strips of aluminum attached to the inner wall of the plexiglass shell serve to accommodate the flat blade tips. In addition, holes have been drilled each quarter inch along the flat sides of the core so that blade spacing can be varied in increments of about twelve per cent of blade chord length.

Each blade is notched at the tip and a hole drilled lengthwise through the blade. The blades are attached to the core by means of bolts which pass through the blade and core wall and are fastened by a nut on the inside wall of the core. The notch in the blade tip which accommodates the bolt head is smoothed over with clay. A cardboard shim having the blade profile is sometimes glued to a blade tip to eliminate blade tip clearance.

Static pressure taps have been provided along the core of the model. The pressure taps are spaced every inch in an axial direction along one of the curved surfaces of the core. The tubing connected to these pressure taps passes through a hole at one end of the rectifier. Static pressure taps are also provided at four inch intervals along the outer plexiglass shell. The static pressure taps are not used during unsteady flow testing.

In order to facilitate insertion of the rectifier into the plexiglass shell, the shell has been split in half lengthwise. This has the further advantage of making the elimination of blade tip clearance easier, since the two halves of the shell can be strapped tightly down against the blades. The supporting structure and the bottom half of the plexiglass shell serve as a cradle for the rectifier. The top half, or lid, of the shell is removed when it is desired to make changes in blade configuration.

STEADY FLOW PERFORMANCE

All steady flow testing was performed in a wind tunnel with a plenum chamber pressure of one psi. The test procedure and experimental results are discussed in the following paragraphs.

The entrance region for restricted flow operation was designed as follows: Some standard NACA airfoil profiles were selected and some blades with about a two inch chord were made. The blades were attached to the core so that the angle of attack varied linearly with axial distance along the rectifier. Mass flow measurements were made for operation in the restricted flow direction and flow patterns were determined visually with the aid of tufts attached to the trailing edges of the blades. Some of the blades were at too high an angle of attack. Accordingly, the angles of attack were changed in succeeding tests in an effort to eliminate blade stall. Blade spacing was also varied in an effort to find the optimum configuration.

It was found that the static pressure decreases more rapidly at the root, that is, along the inner core, than at the tip. This was to be expected, at least near the entrance region, because of the transition from axial to helical flow. It also accounts for the fact that more camber was needed to prevent stall at the blade tip section than at the root. Because of the observation that more camber was needed at the tip in the intermediate range between transition from axial to helical flow, flaps were attached to some of the blades to prevent blade tip stall. The blades with flaps attached can be seen in some of the figures showing photographs of the rectifier and a close-up photograph is shown in figure 7. The flap is tapered so that it provides a maximum effective camber at the tip section.

The overall blade configuration, which is specified in Table 1, was chosen in the following manner: The entrance blades, for restricted flow operation, were selected on the basis of what was learned from the series of tests described above. The blades in the transition section between the entrance region and the cascade column of 90° turning blades were chosen as a compromise between the two extreme types. Two of these blades were obtained by modifying 90° turning blades as shown in figure 8. The cascade section consisted of 90° turning blades, designed for a solidity of 1.63.

After a few preliminary tests, mostly of a qualitative nature, five tests were run using different blade column lengths. The results are summarized graphically in figure 9. Two significant points can be made from an examination of figure 9. First, frictional effects are rather severe. In fact, the loss due to friction in the free flow direction reduces the overall performance by 25 per cent when operating with a total pressure drop of one psi. Secondly, the performance is quite dependent on the number of 90° turning blades used in the cascade section. It appears from the slope of the performance curve that significant improvement could be obtained merely by adding a few more 90° turning blades. This was not done because of limitations imposed by the model length unless extensive changes were to be made.

Figure 10 shows the radial variation in total and static pressure at four points along the rectifier axis (specified by corresponding blade position), and along a radial line 60° from the trailing edges of a blade column. The flow is strongly rotational in this region as can be seen from the large radial variation in total pressure. The static pressure is only approximate. Nevertheless, it confirms the observation that most of the air flow seemed to be near the outer plexiglass shell, for the figure indicates that the dynamic pressure, as well as the total pressure and static pressure, is greater near the outer shell than the inner core. Figure 11 is a cross plot of the data presented in figure 10. It shows the variation in pressure with axial distance. Finally, figure 12 gives an indication of the streamlines in the same region as that in which the pressure surveys were made. The arrows indicating flow paths were obtained from a yaw survey.

From the plot of the streamlines in figure 12, it is evident that the flow enters the cascade columns at a reasonable angle of attack. Hence the 90° turning blades are able to perform as designed rather than to just provide resistance for detached flow. While figure 9 indicates increased performance with addition of 90° turning blades, it is to be expected that a limit would soon be reached. The limit would correspond to the point where increased frictional resistance in free flow offsets the increase in performance due to addition of 90° turning blades. However, if more 90° turning blades were added, so as to at least resist the flow more in the restricted flow direction, it might be possible to shorten the entrance region and reduce free flow friction. Certainly, there is much that can be done to better the present performance. In particular, the proper blade design for the transition section needs attention. This section was not studied in great detail except to note that the blades did not perform as well there, as indicated by trailing edge tufts, as in either the entrance or 90° cascade section.

UNSTEADY FLOW PERFORMANCE

The model used for unsteady flow testing utilized the blade configuration described in Table 1, but had only 18 blades per column. The last two 90° turning blades were broken off at too late a date for replacement. The steady flow performance coefficient is about 7.5 for the model used in all unsteady flow testing.

Figure 13 presents an illustration of the test stand and associated instrumentation. A cellophane diaphragm is clamped over the exit of the rectifier (figure 6) and the entire system is pressurized to one psi. The cellophane diaphragm is punctured and the pressure variation at point A or B, as illustrated in figure 13, is detected by a quartz pressure transducer, having a natural frequency of 48,000 cps with high damping. The event is recorded with the aid of an oscilloscope and camera. A single sweep of the oscilloscope is synchronized with the event and is triggered simultaneously with the rupturing of the diaphragm.

Many tests were run for both free flow and restricted flow directions. The pressure variation was recorded over long time intervals to get the overall structure and over short intervals to obtain more detail in certain regions. A few typical results are shown in figures 16 to 19. Figures 20 through 22 show reproductions of the pressure variation for each type of experiment. Each of these figures has been obtained by an analysis of the results of several experiments. An attempt has been made to show the arrival of distinct pressure waves or expansion waves. However, the overall shape and the sharp drops in pressure due to the arrival of expansion waves from the end of the rectifier are the only features which are definitely conclusive.

The mass flow lost for both free flow and restricted flow operation is presented graphically in figure 23, and the method of calculation is discussed in Appendix I. There are two salient features to be noted from the graphs presented in figure 23. First, the starting interval, that is, the time required for the aerodynamic rectifier to begin performing as a rectifier, is about 16 milliseconds after the diaphragm has been ruptured. This corresponds to a time of about 12 milliseconds after the arrival of the first wave at the first turning blade and compares well with the starting time determined by another method which will be discussed below. Second, the mass flow during the starting interval is nearly the same as that in the free flow direction for the same time interval. This is just that mass flow expected for the discharge of compressed air from a duct having the dimensions of the test stand shown in figure 13.

Figure 22 presents the pressure as measured at point A in figure 13, but with the duct formerly between the pressure vessel nozzle and rectifier now removed. No analysis has been made since it proved too difficult to interpret the pressure variation at the exit of the nozzle due to the superposition of too many waves. However, the results at point A indicate the same performance as with the duct inserted, except for a difference in timing because of the shorter length of the test stand.

An independent and more direct determination of the starting time was made with a low pressure shock tube test. Figures 14 and 15 are schematics of the shock tube and equipment used. For this test, the nozzle on the pressure vessel was removed and a cellophane diaphragm inserted at the outlet from the pressure vessel. Air was pumped into the pressure vessel until the diaphragm ruptured. As the resulting shock wave passed by the first of three pressure transducers, a single sweep of the oscilloscope was triggered. The pressure was then recorded as measured by the second transducer slightly ahead of the rectifier, and simultaneously by the third transducer slightly behind the rectifier. The length of tube between the pressure vessel and rectifier was of sufficient length to permit the development of a fairly sharp shock wave. The tube length downstream, which had a closed end to reduce noise, was long enough to provide time for steady state conditions to develop through the rectifier before the arrival of the reflected pressure wave from the tube end.

A typical result of the preceding tests is shown in figure 26, and is discussed at greater length in Appendix II. The essence of the test is that it takes about 14 milliseconds to reach steady state operation after the arrival of a weak shock wave at the first turning blade. This is in good agreement with the starting time as determined by tests discussed earlier in this chapter.

TABLE I

Blade Configuration for Kantrowitz Type Rectifier

Blade No.	Blade Spacing	Angle of Incidence*	Blade Type**
1	3.25"	12°	A
2	3.00"	22°	A
3	2.75"	30°	B
4	2.50"	38°	C
5	2.25"	45°	C
6	2.25"	50°	C
7	1.75"	70°	E
8	1.50"	85°	F
9	1.25"	90°	D
10 - 20		90°	D

* Angle of incidence is defined as the angle the chord line, drawn from leading edge to trailing edge, makes with respect to the free flow stream direction.

** See figures 7 and 8.

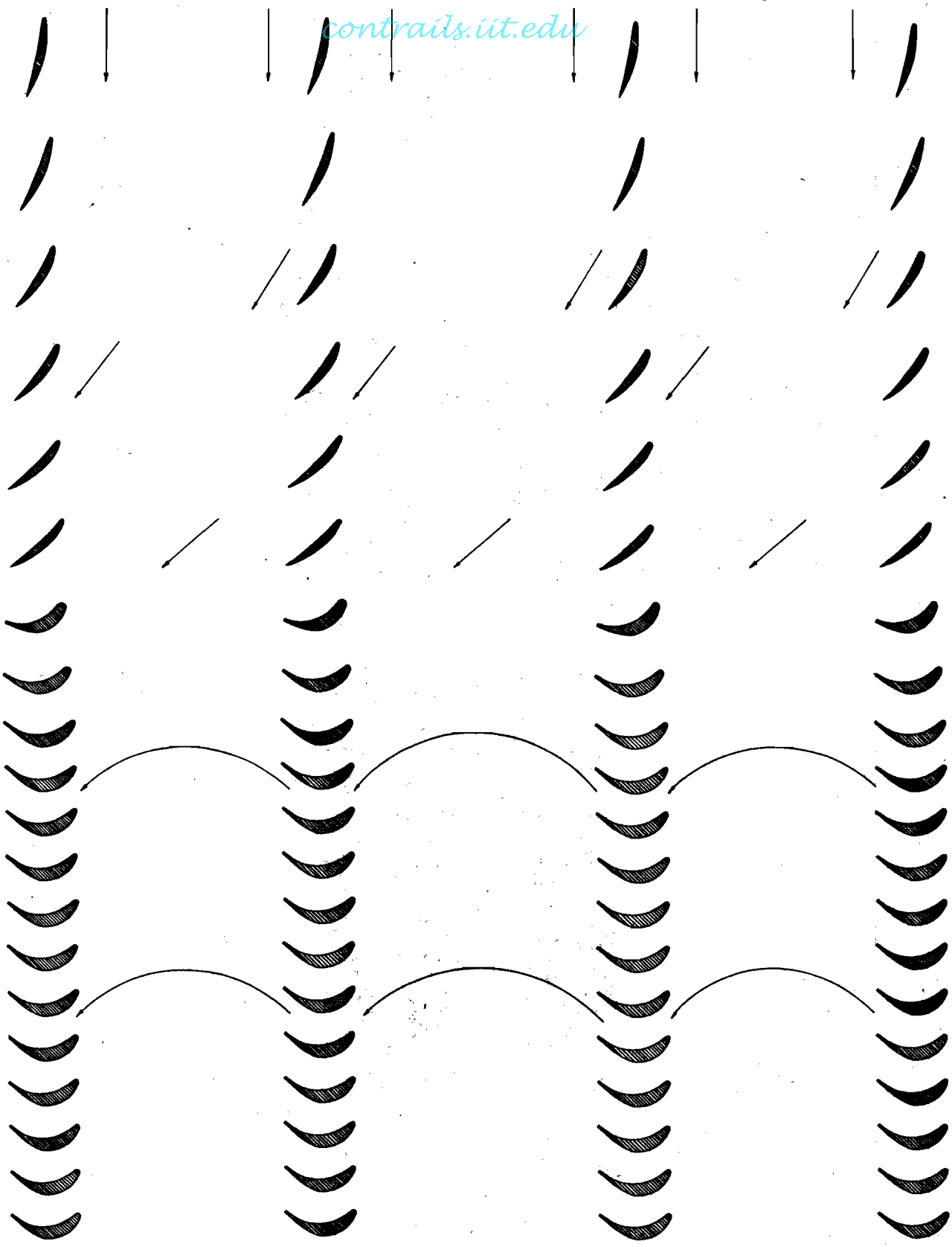

Figure 1. Developed View of Blade Configuration Showing Ideal Flow Pattern.

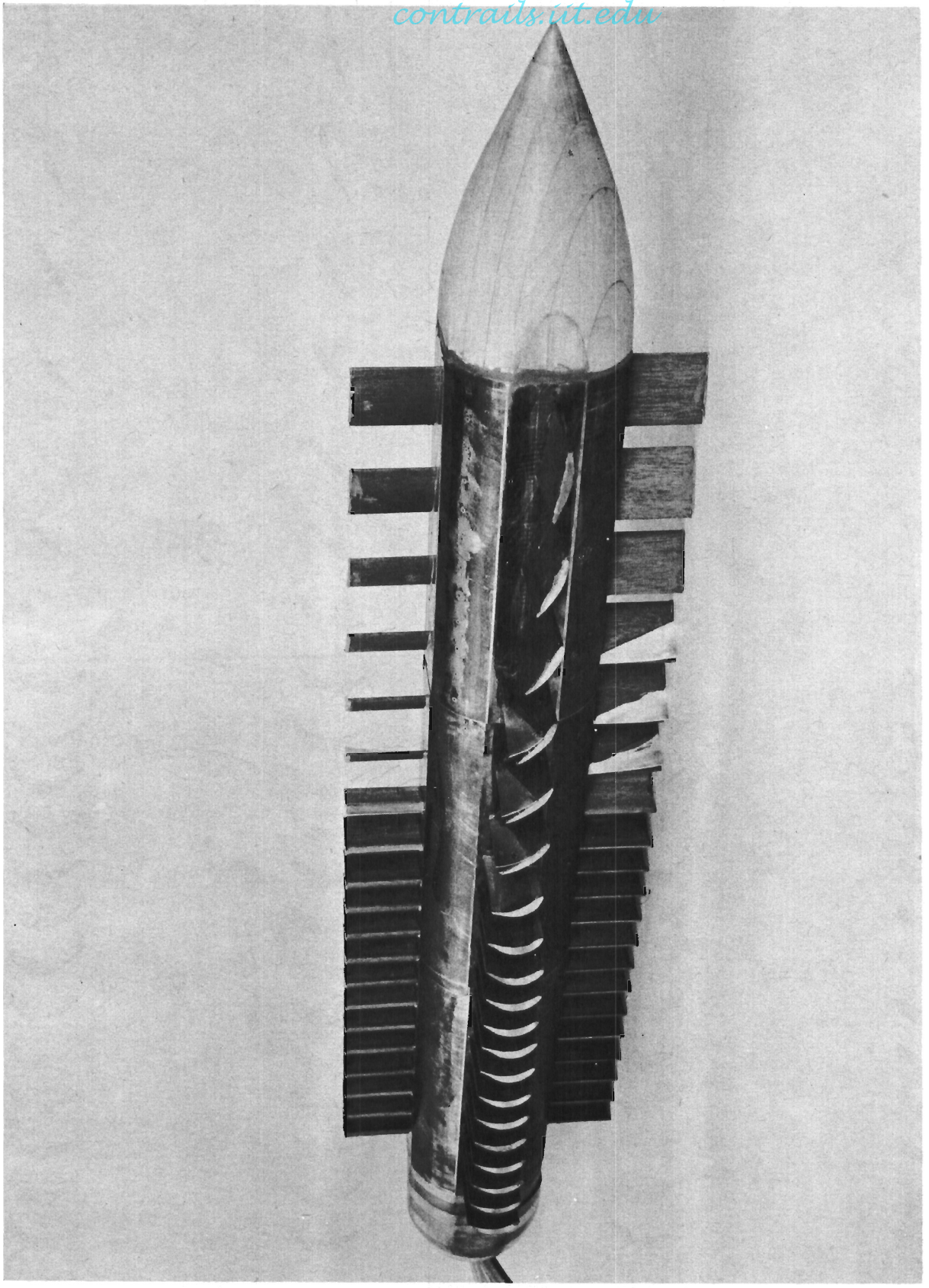

Figure 2. Aerodynamic Rectifier.

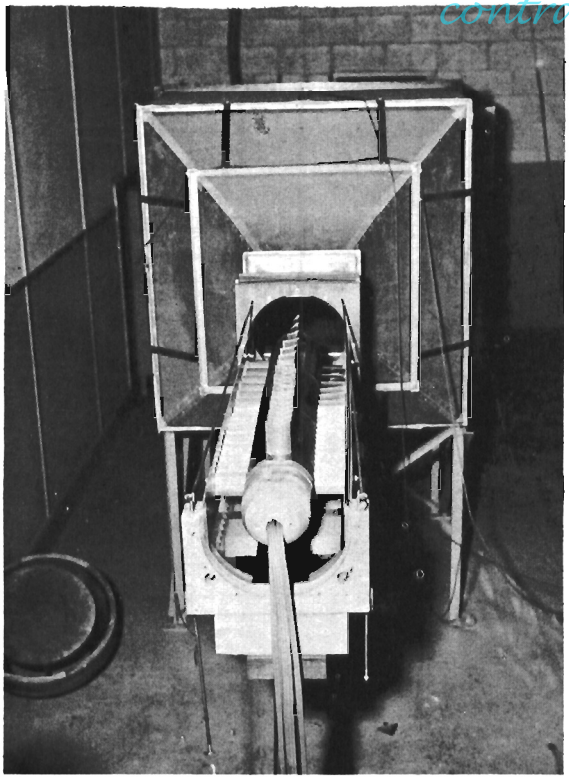

Figure 3. Aerodynamic Rectifier Supported in Cradle of Wind Tunnel Test Stand.

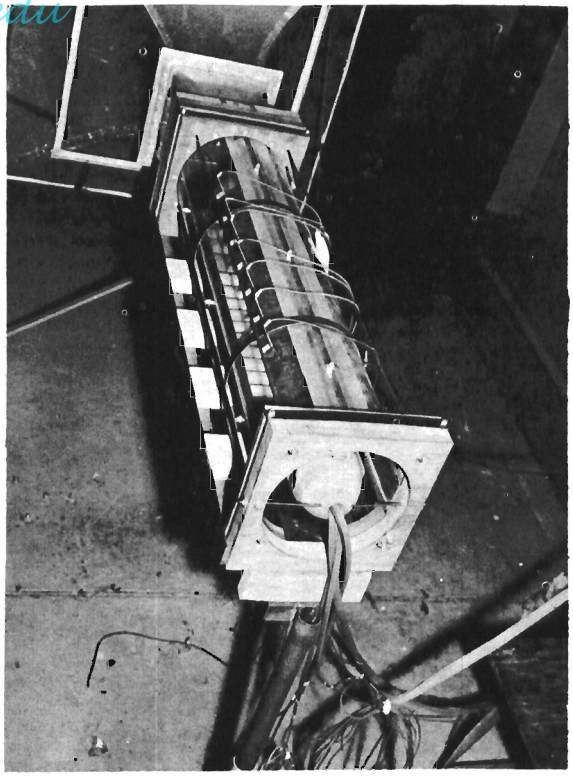

Figure 4. Aerodynamic Rectifier Enclosed in Plexiglass Shell and Ready for Wind Tunnel Testing.

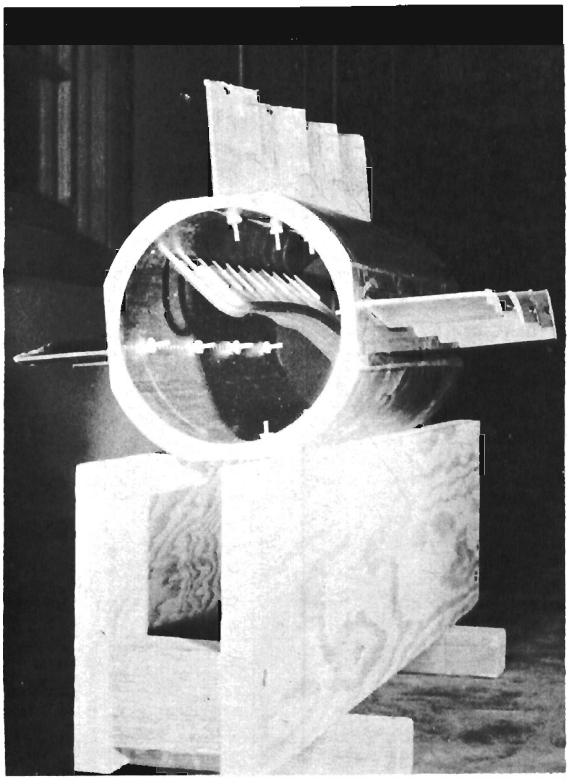

Figure 5. Section of Core of Aerodynamic Rectifier Showing Method of Blade and Tubing Attachment.

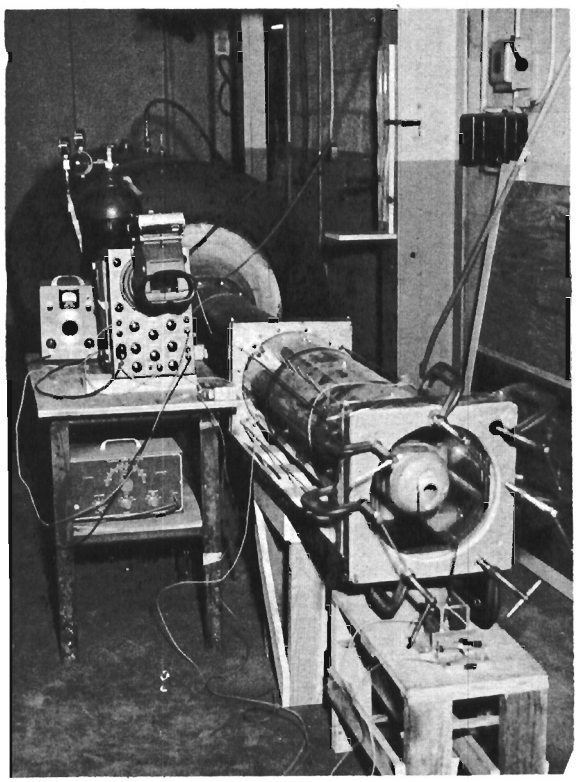

Figure 6. Aerodynamic Rectifier Unsteady Flow Test Stand.

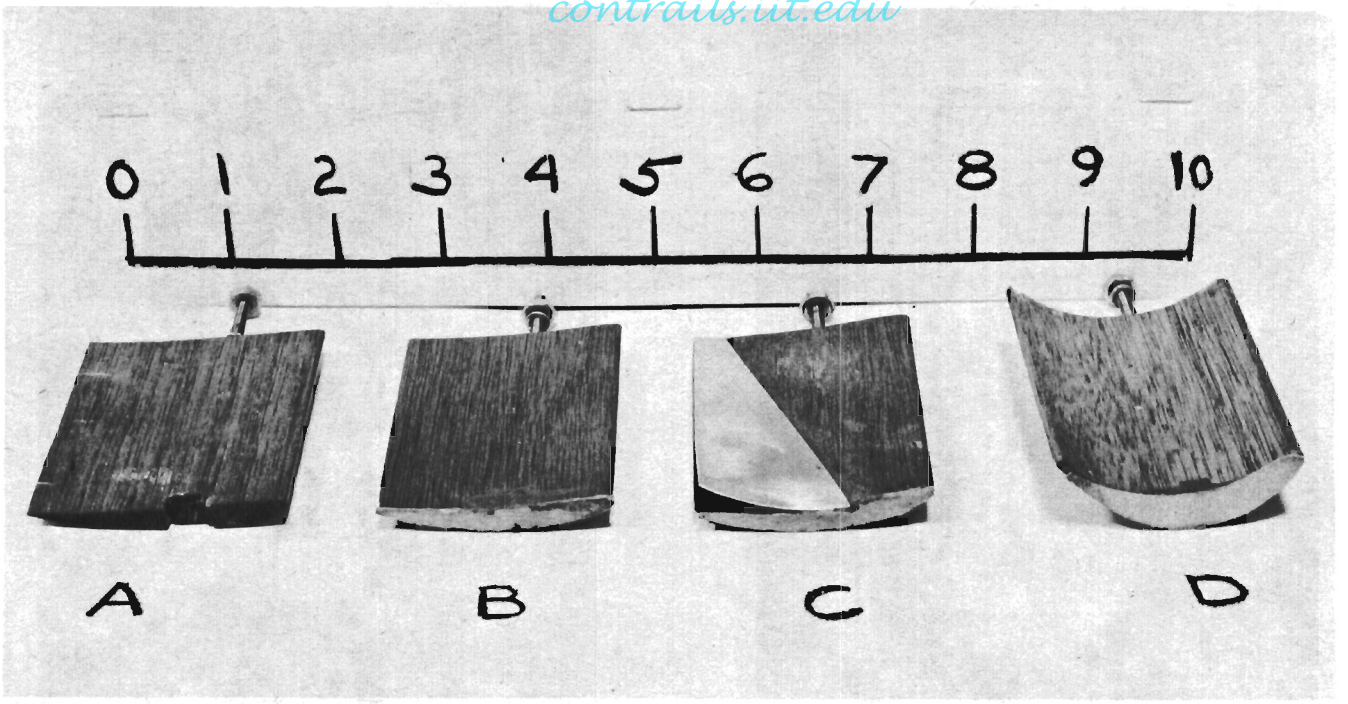

Figure 7. Turning Blades.

A NACA 6510-64 Profile
B NACA 7512-64 Profile
C NACA 7512-64 With Flap
D 90° Turning Blade

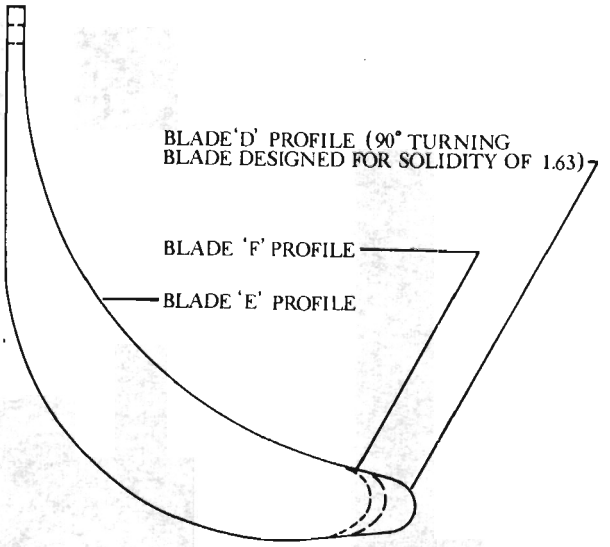

Figure 8. Blade Profiles.

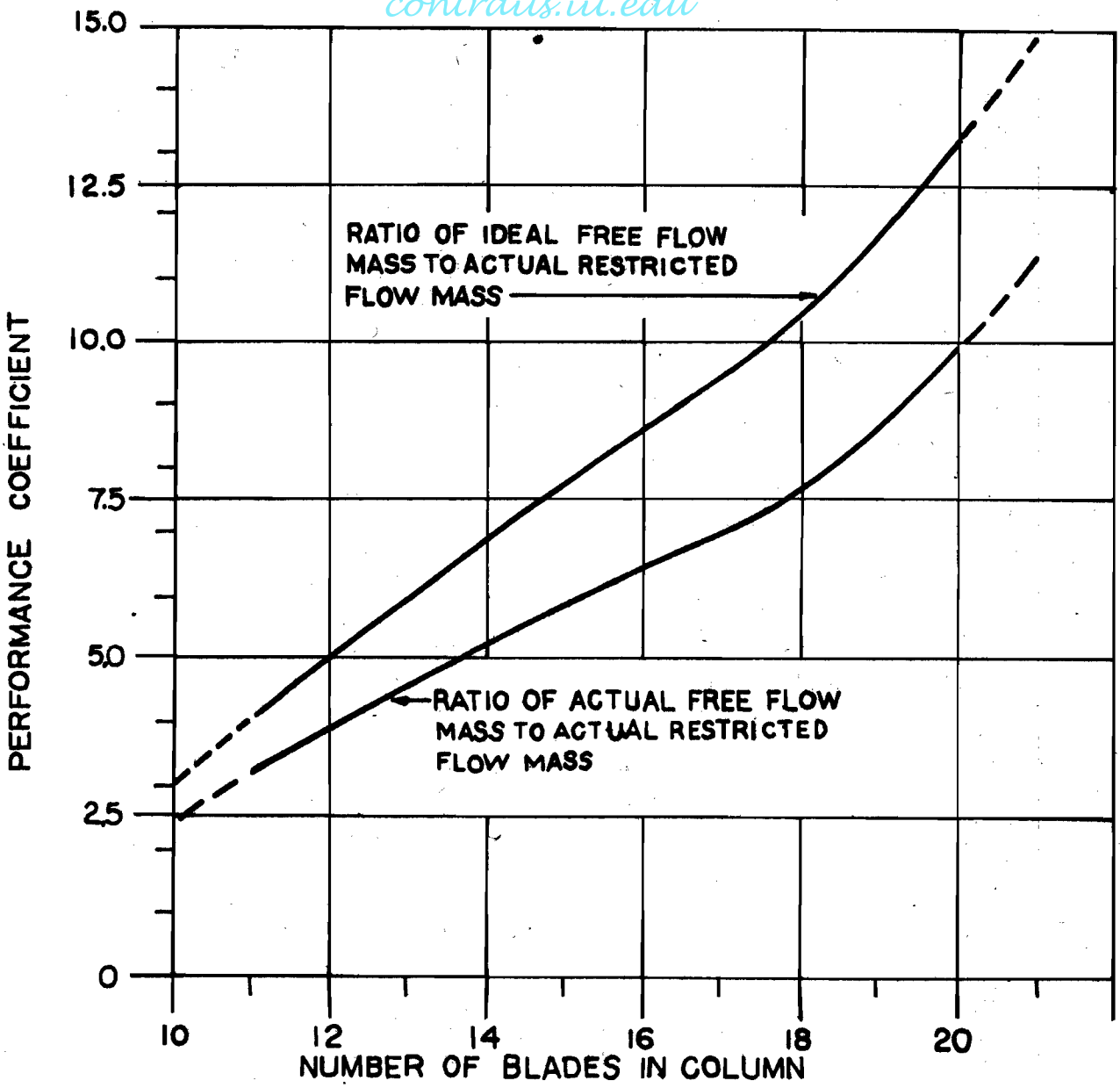

Figure 9. Performance Coefficients.

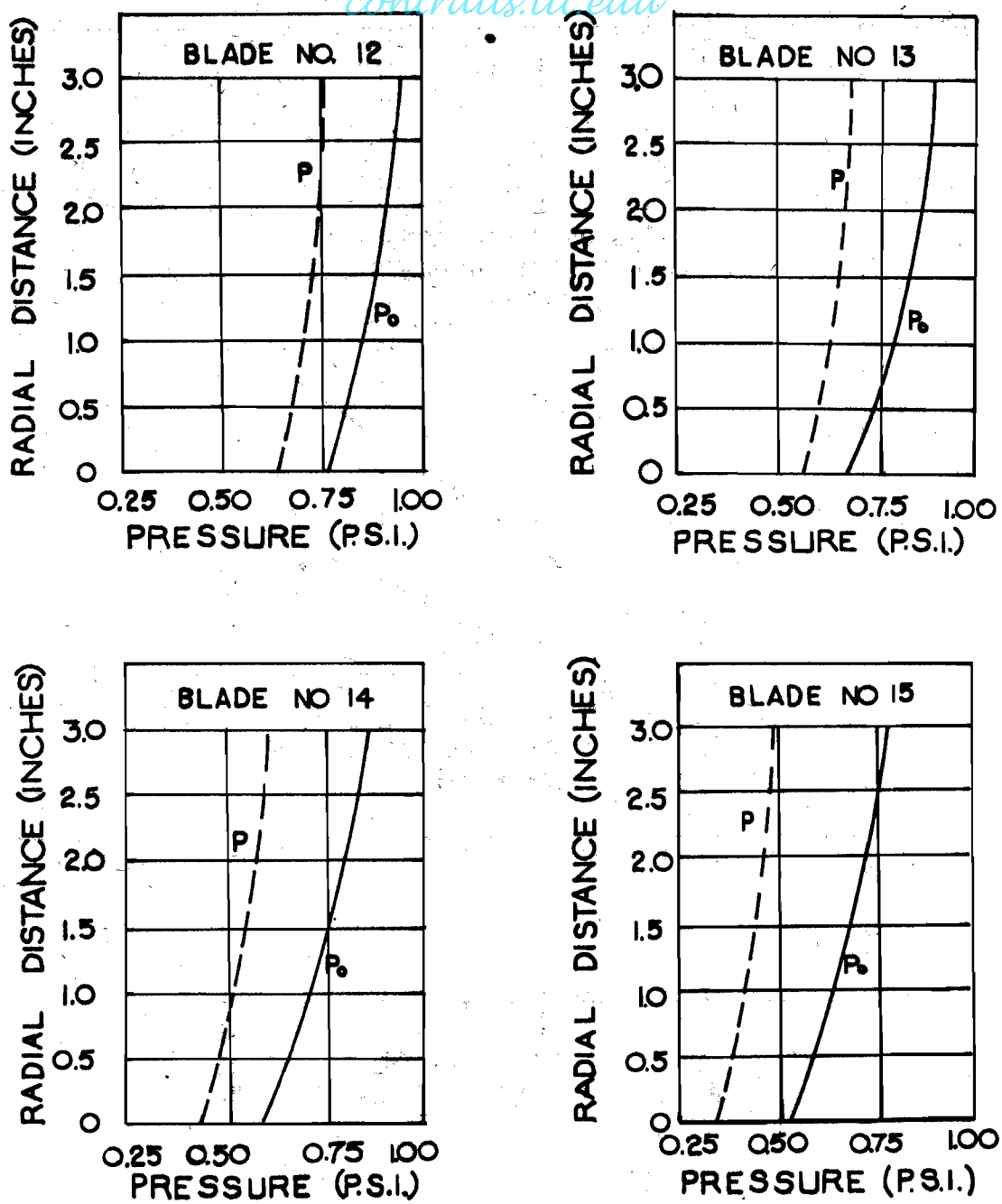

Figure 10. Pressure Profiles.

Total pressure (P_o) and static pressure (P).
Profiles are along radial lines 60° from the trailing edges of a blade column.

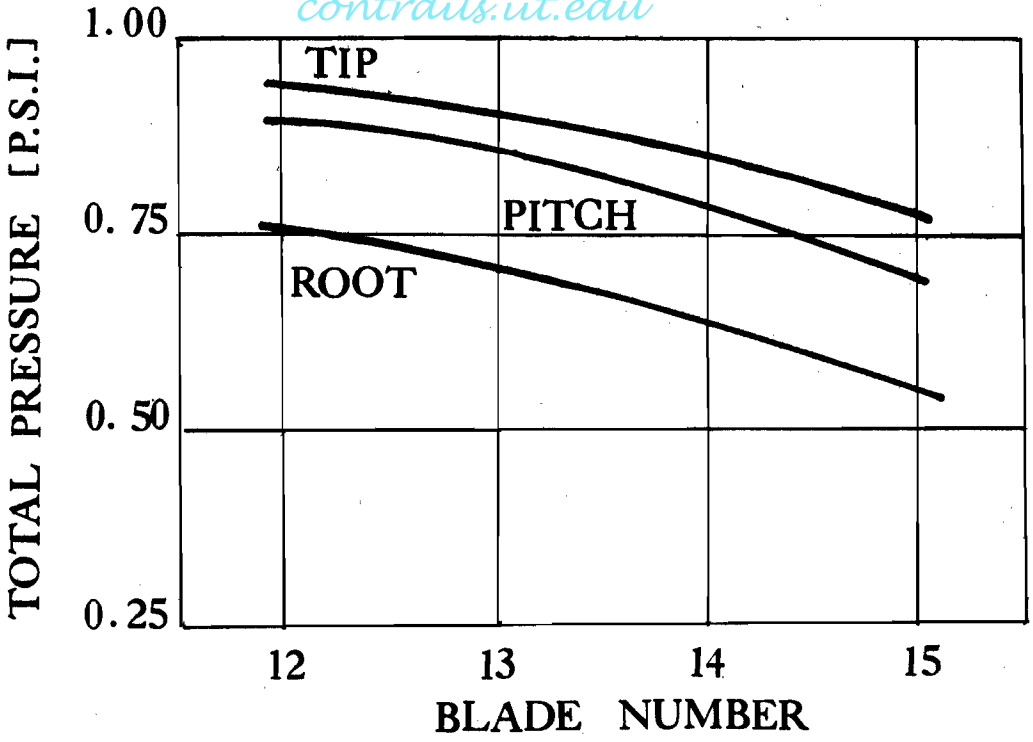

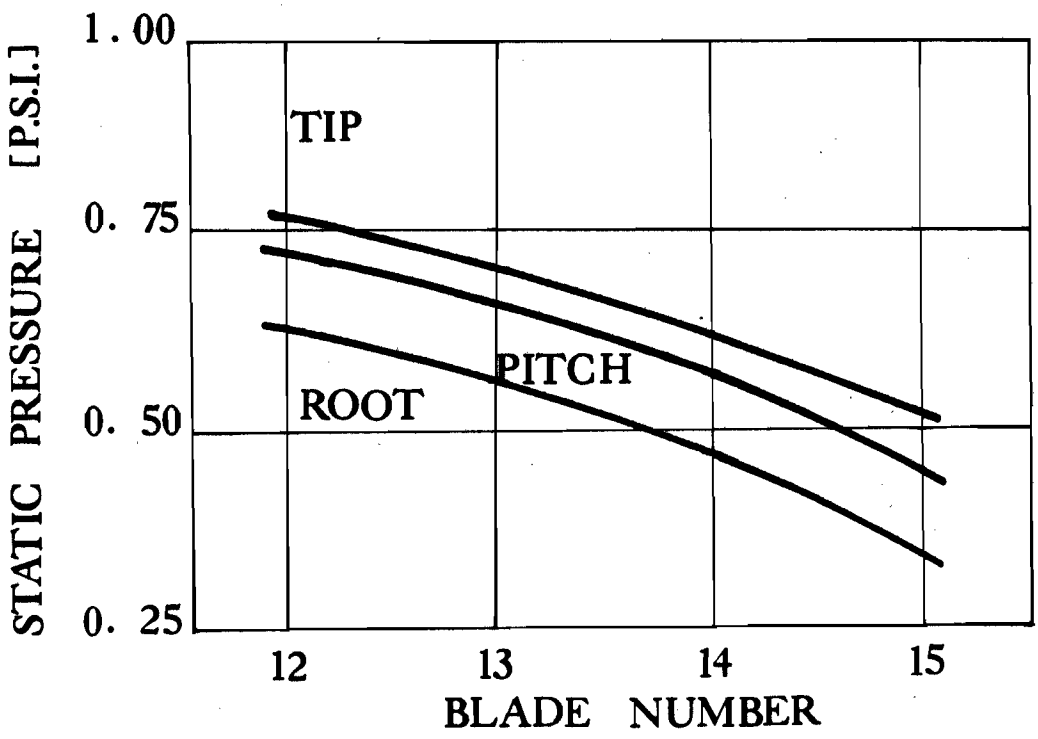

Figure 11. Pressure Profiles

Profiles are along a plane passing through the axis of the rectifier and 60° from the trailing edges of a blade column.

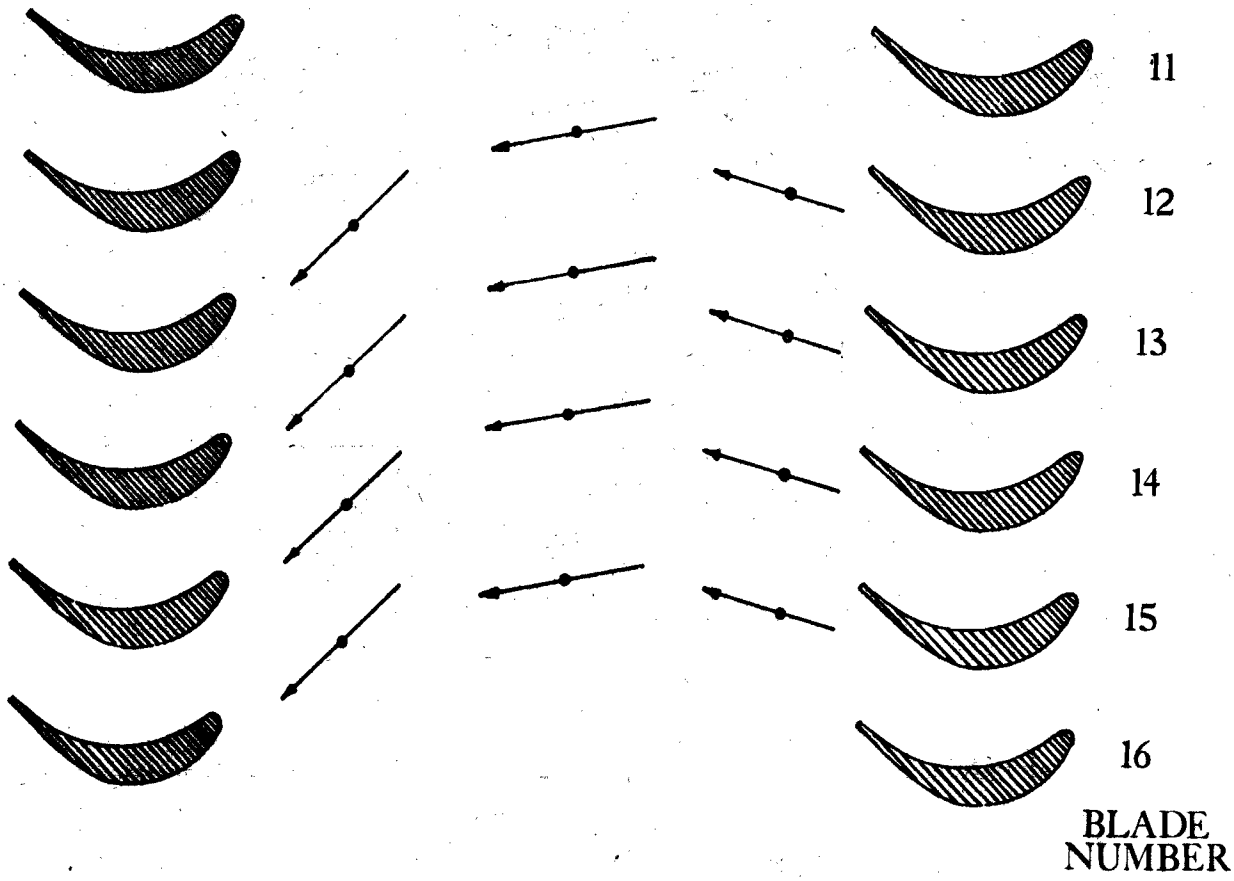

Figure 12. Approximate Flow Pattern in 90° Turning Blade Cascade Section.

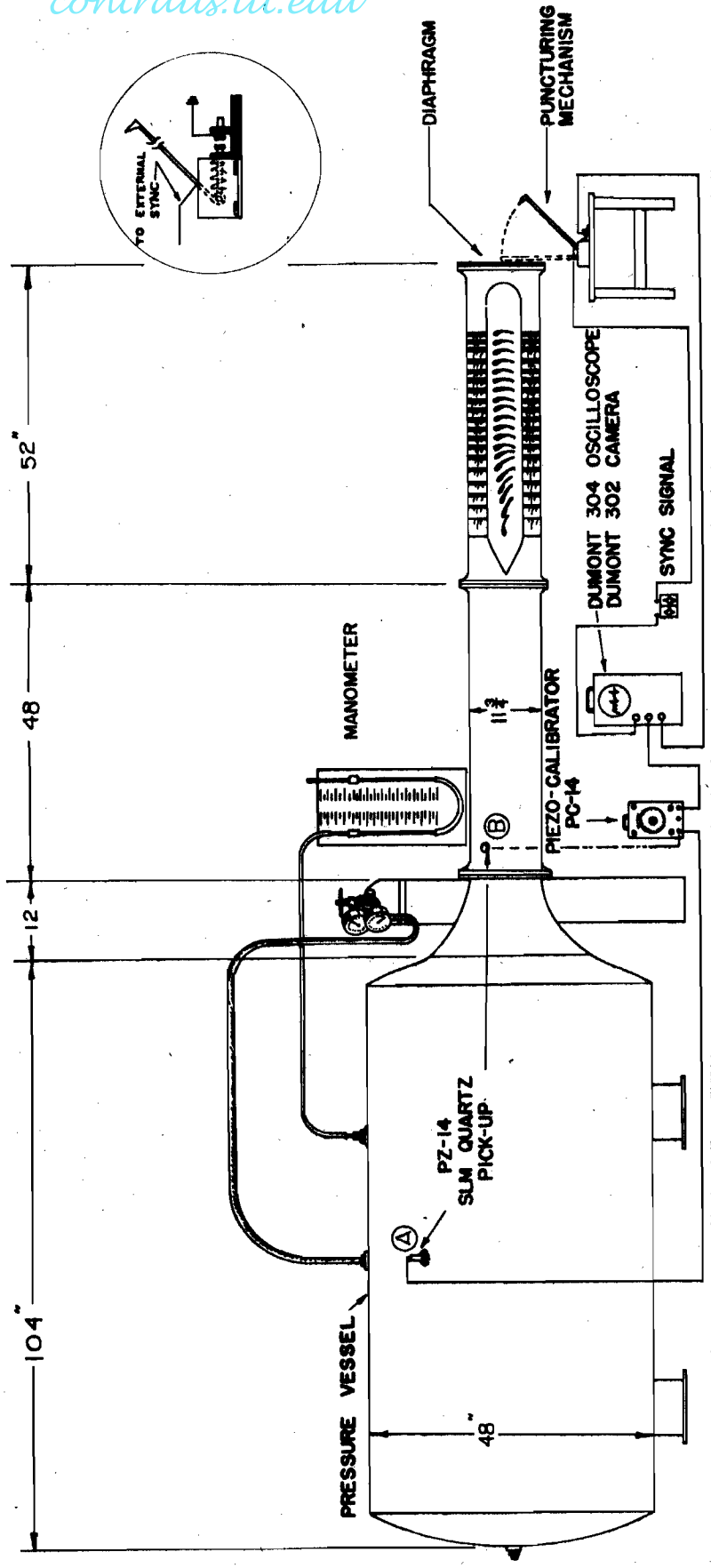

Figure 13. Unsteady Flow Test Installation.

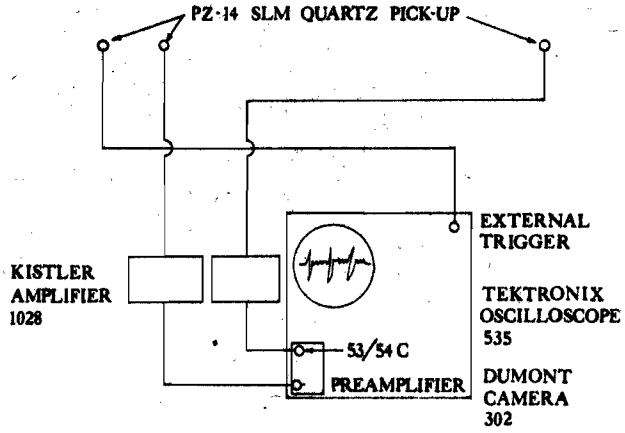

Figure 14. Instrumentation for Shock Tube Installation.

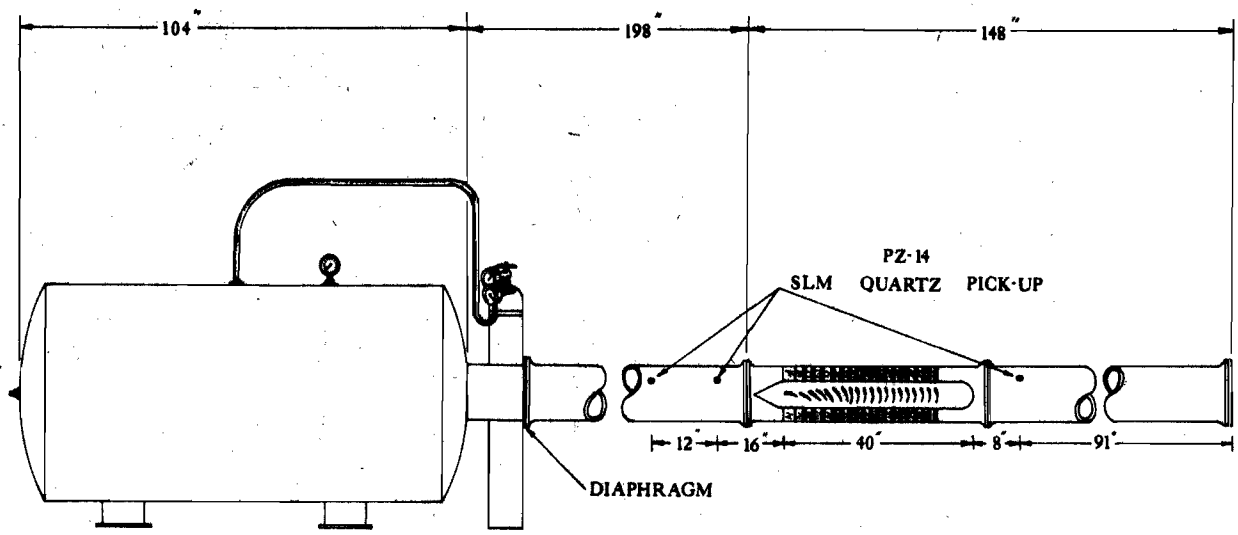

Figure 15. Shock Tube Installation.

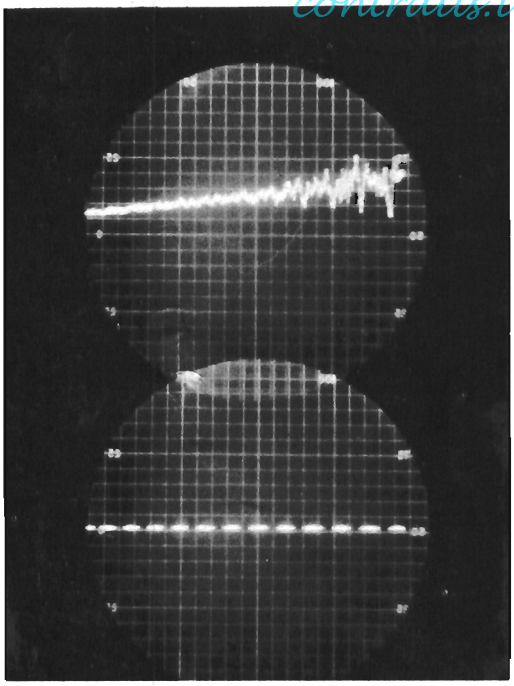

Figure 16. Point B:
Restricted Flow Pressure
Variation.

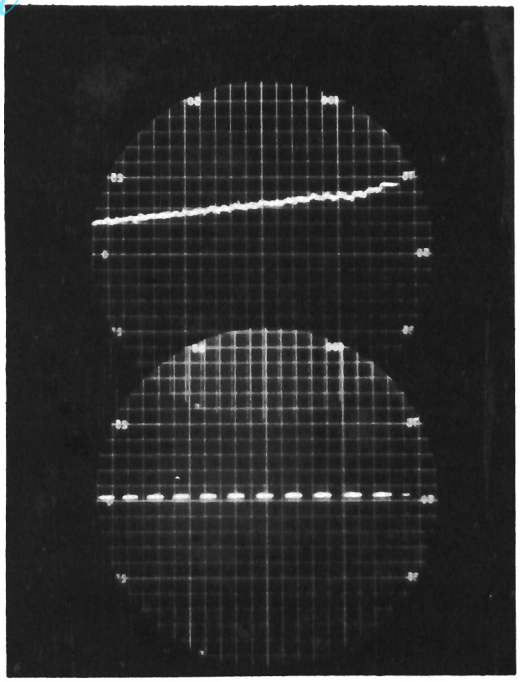

Figure 17. Point A:
Restricted Flow Pressure
Variation.

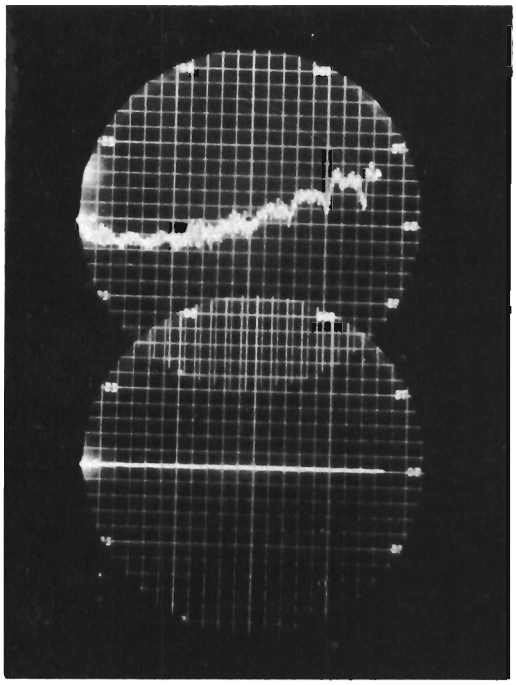

Figure 18. Point B:
Free Flow Pressure Variation.

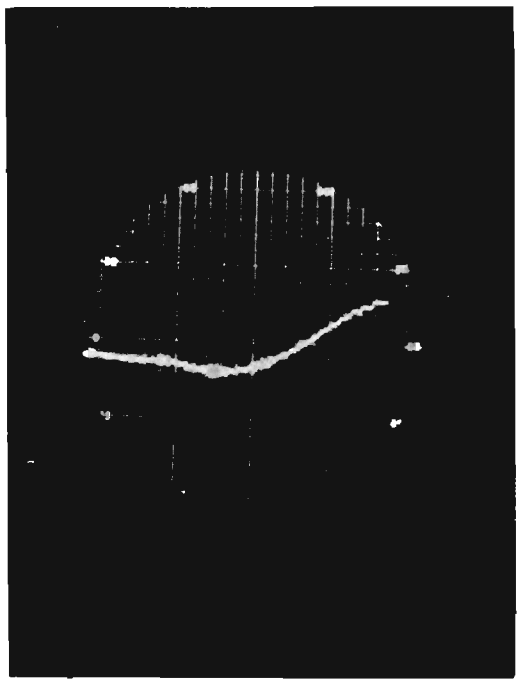

Figure 19. Point A:
Free Flow Pressure Variation.

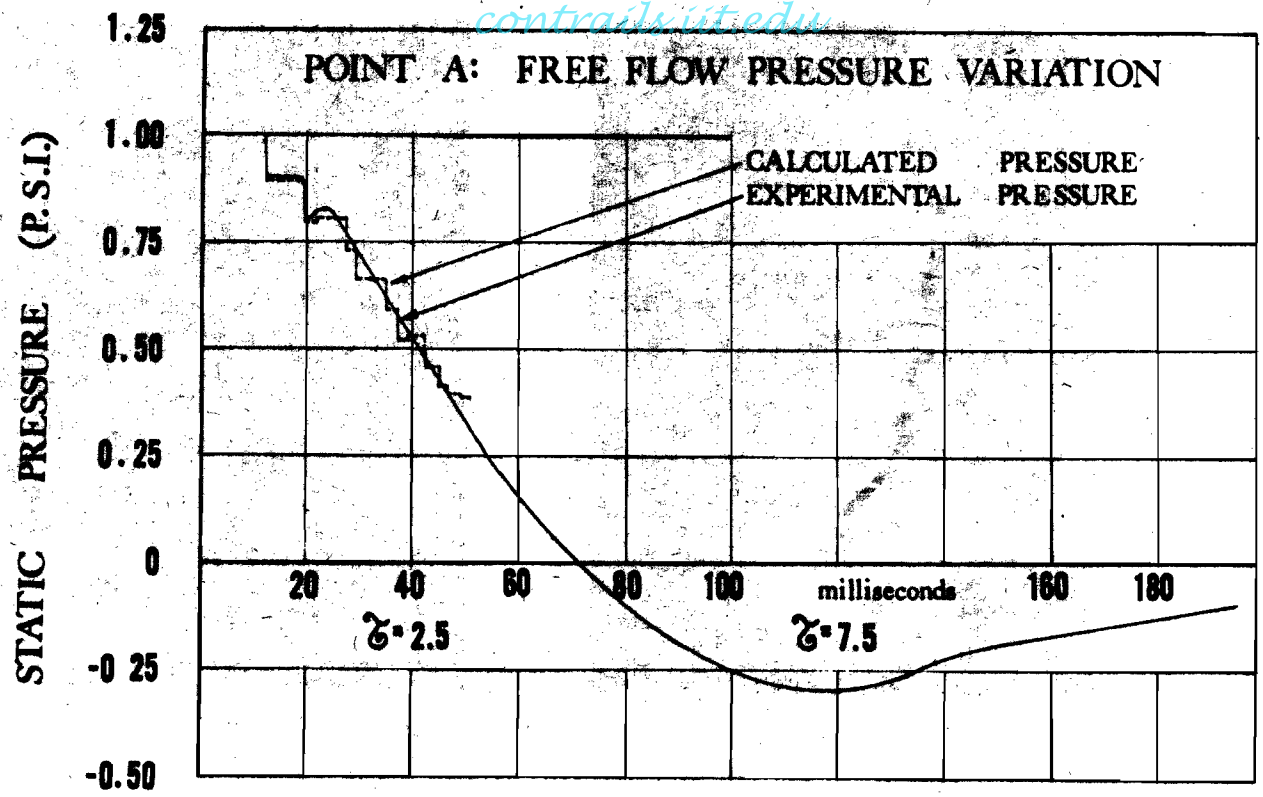

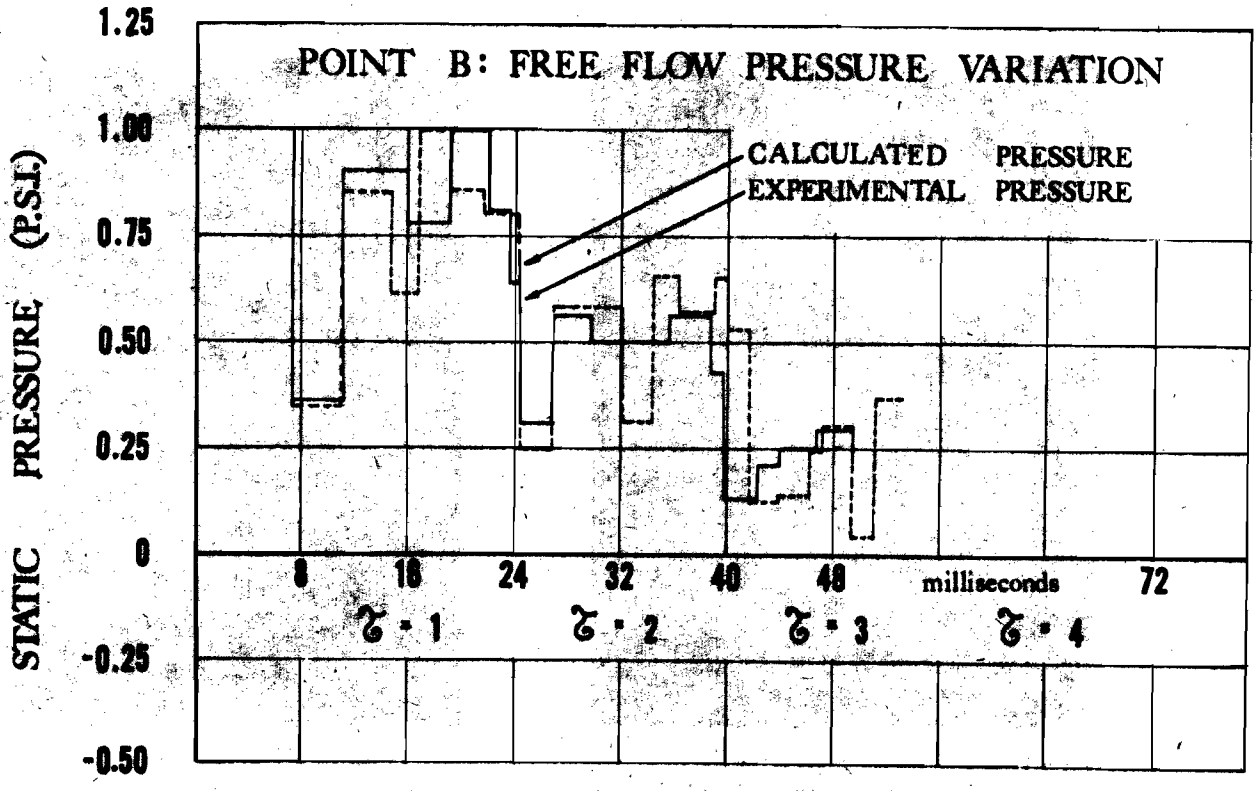

Figure 20. Free Flow Pressure Variation.

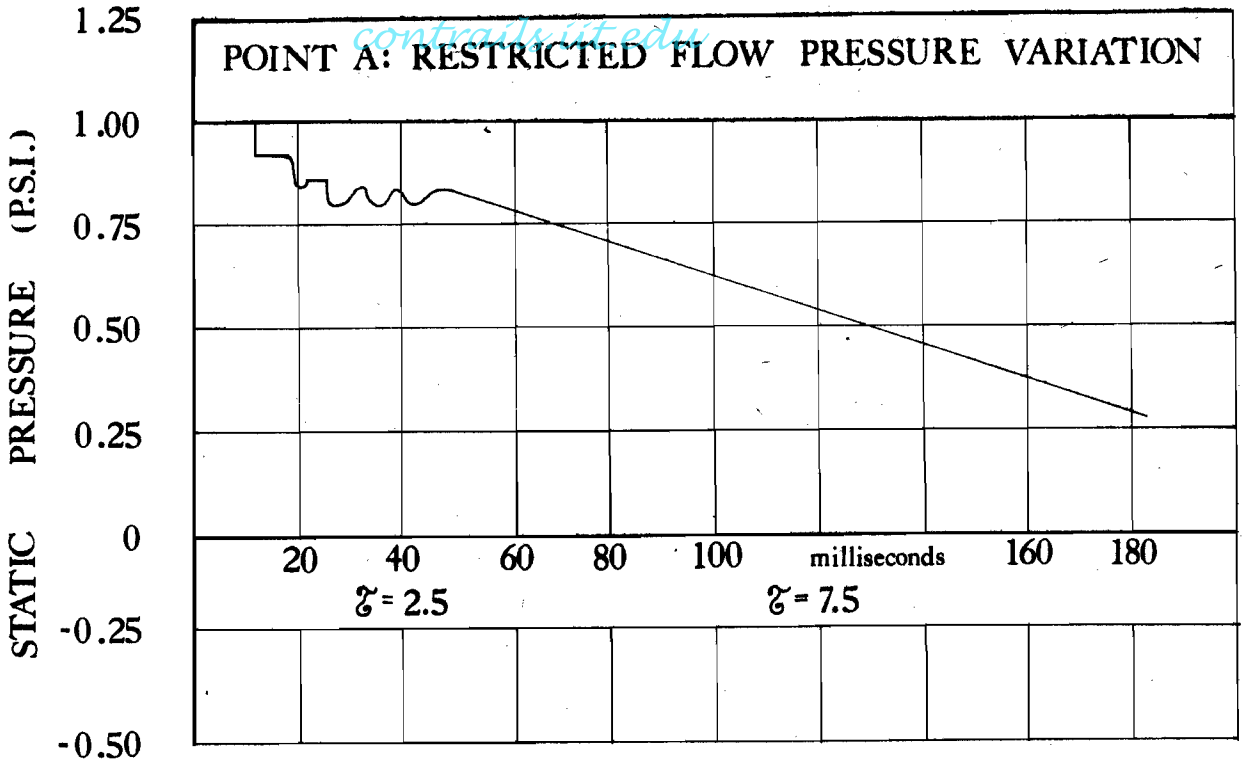

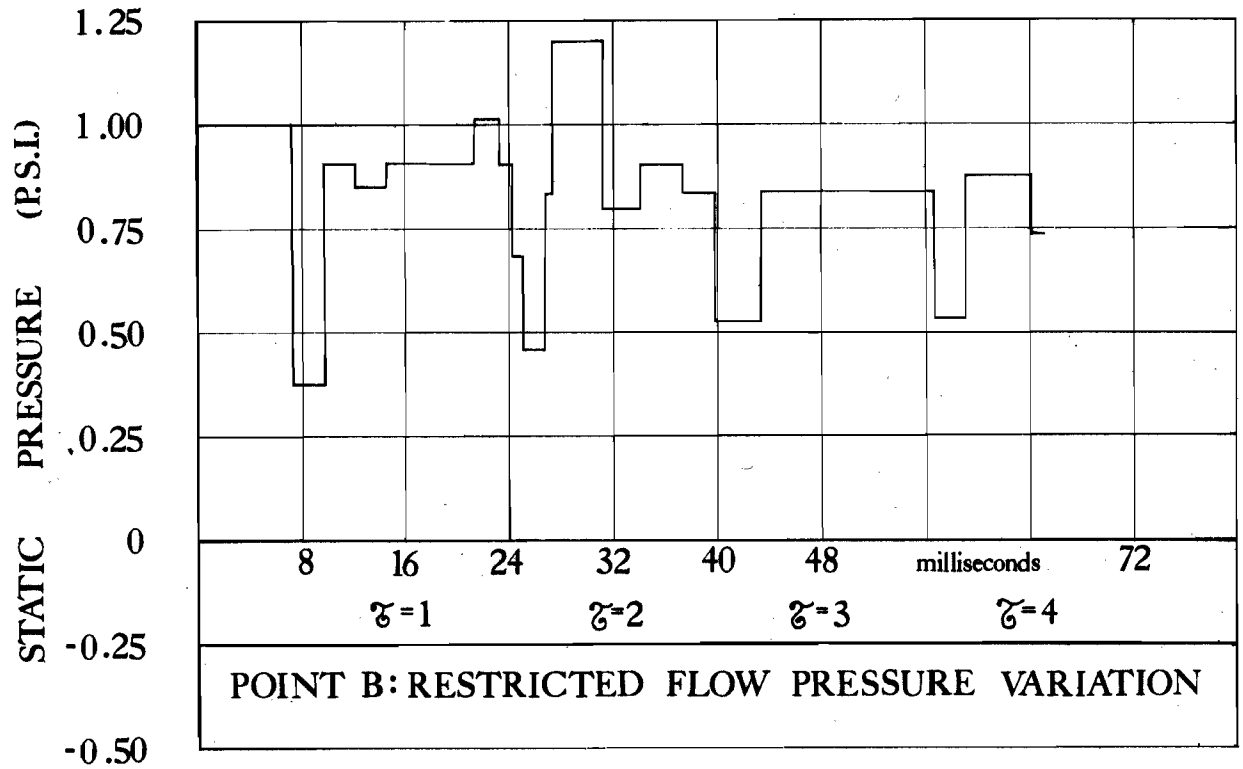

Figure 21. Restricted Flow Pressure Variation.

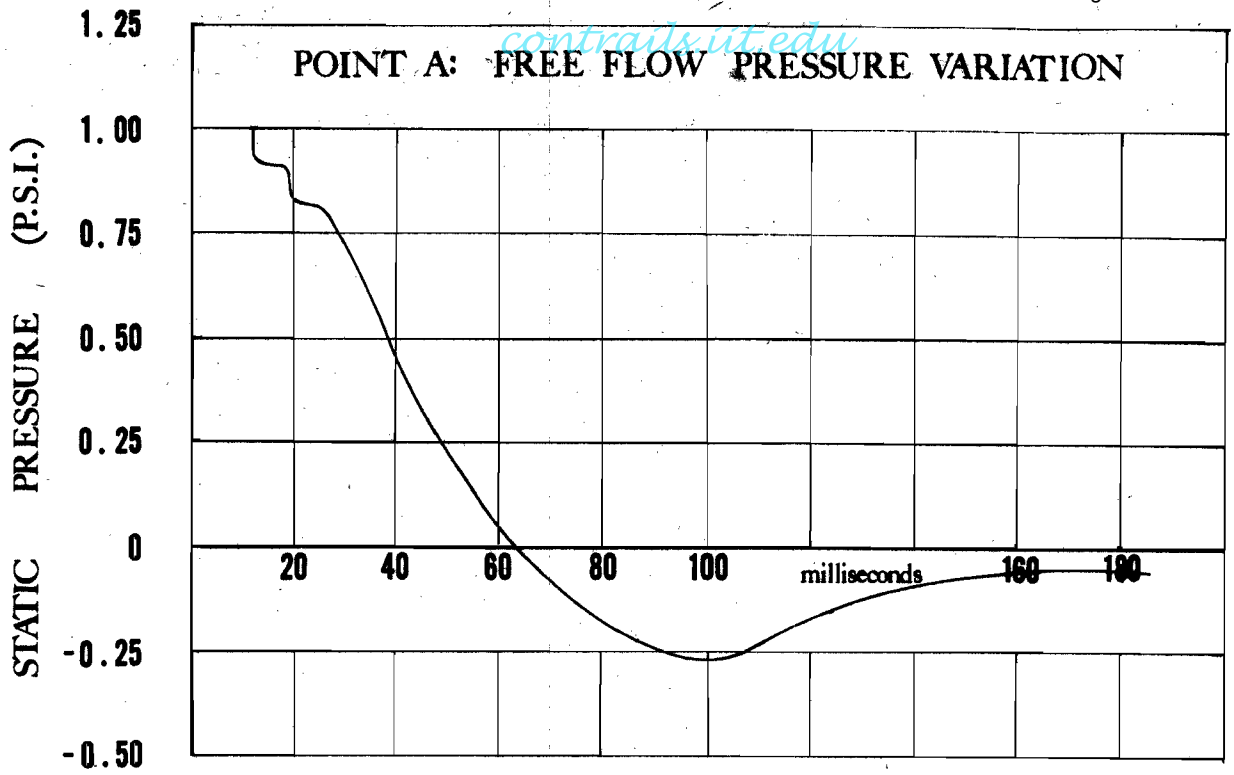

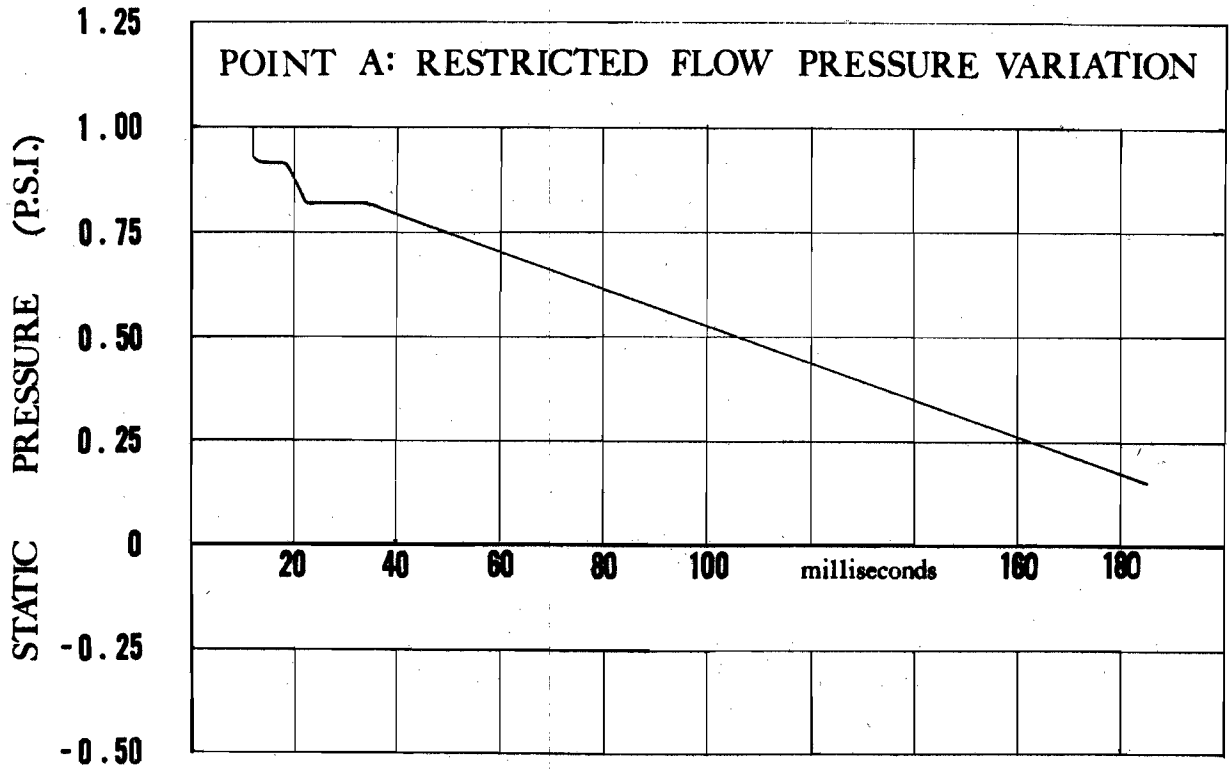

Figure 22. Pressure Variation for Unsteady Flow Test Installation with Duct Removed.

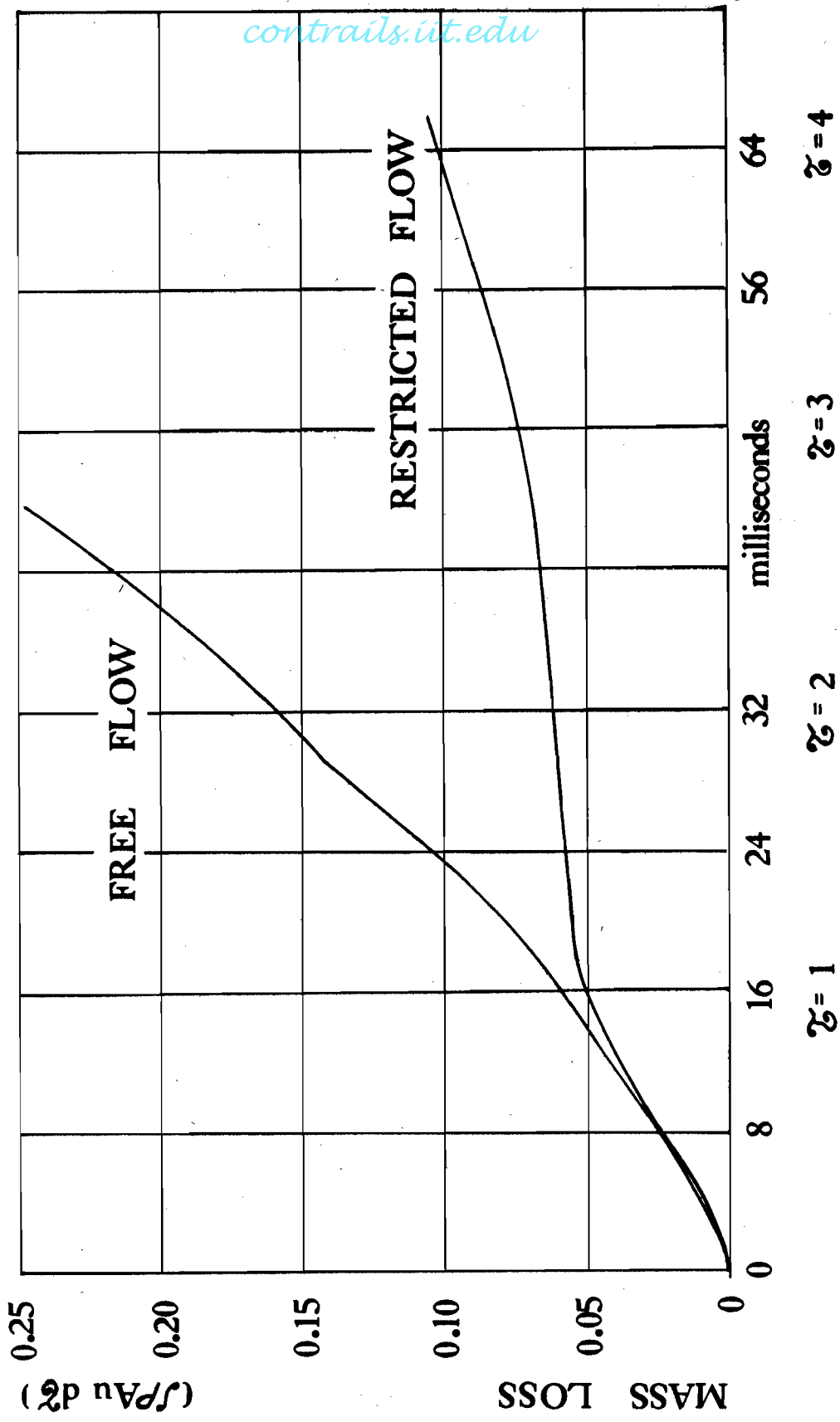

Figure 23. Mass Flow Loss for Unsteady Flow Operation.

BIBLIOGRAPHY

1. Tesla, N., Valvular Conduit, U.S. Patent No. 1,329,559, 3 February 1920.

2. Wislicenus, G.F., Flow Control Means for Pulse Jet Combustion Units, U.S. Patent No. 2,618,925, 31 January 1947.

3. Schultz-Grunow, Gas-Dynamic Investigation of the Pulse-Jet Tube, Parts I and II, NACA TM 1131, February, 1947.

4. Linderoth, E.T., Aerodynamic Check Valve, U.S. Patent No. 2,727,535, 17 January 1950.

5. Bertin, S., Principles de Fonctionnement du Pulso-Reacteur, AGARD Report, 1953.

6. Kantrowitz, Arthur, An Aerodynamic Valve, All American Engineering Company Report No. M-162, 8 November 1954.

7. Rudinger, George, Wave Diagrams for Nonsteady Flow in Ducts, D.Van Nostrand Company, Inc., New York, 1955.

8. Wooten, Frederick O., Design and Performance of an Aerodynamic Rectifier Under Steady Incompressible Flow Conditions, WADC TN 56-359, September, 1956.

APPENDIX I

DETERMINATION OF UNSTEADY FLOW PERFORMANCE

Unlike the case for steady flow conditions, the unsteady flow performance is not as readily obtained from the experimental data. In general, recourse must be made to the method of characteristics and the use of wave diagrams. References 3 and 7 have been used as sources of information on the techniques of wave diagram construction.

The mass flow for operation in the restricted flow direction has been found from the measured pressure variation in the pressure vessel. Figure 21 shows the pressure variation used for the calculations. First, the mass lost from the pressure vessel itself is found. Expressed in nondimensional form and assuming isentropic flow, the mass lost is given by

$$V(\rho_i - \rho) = V(p_i^{5/7} - p^{5/7})$$

where V is the volume of the pressure vessel. The mass flow loss through the rectifier is then found by modifying the mass lost from the pressure vessel in such a manner as to account for the fact that there is a significant discontinuity in cross-section in passing from the duct to the pressure vessel. That is, the initial incoming expansion wave is reflected from the pressure vessel and further accelerates the flow in the duct. Simultaneously, the chamber pressure drops to a pressure corresponding to the greater velocity and not to the initial velocity through the rectifier. After the passage of several waves the pressure does not change so much and the correction becomes negligible. A check on the method is provided since the pressure variation for the passage of the first few waves is nearly the same for either flow direction. Hence, the mass flow for the free flow direction, which will be discussed shortly, can be used for the first few wave passages with restricted flow.

The mass flow for operation in the free flow direction is not directly comparable with the restricted flow direction. This is because the pressure vessel is much too small to maintain a sufficient back pressure when the aerodynamic rectifier is operating in the free flow direction. In fact, as is seen in figure 20, the pressure quickly drops to below atmospheric pressure. What needs to be done is to calculate the mass flow in the free flow direction, assuming the pressure variation in the pressure vessel to be the same as that for restricted flow.

The entire system, consisting of pressure vessel, nozzle, ducting, and aerodynamic rectifier, is treated as a duct of variable cross-section. The duct is closed at one end and suddenly opened to the atmosphere at the other end. It is assumed that the flow is isentropic and that the idealized duct can be approximated by two stepwise changes in cross-section. A wave diagram has been constructed (figure 24), for the test stand configuration of figure 13, with an initial pressure of one psi for free flow operation. Table II lists the properties for each of the states shown in the wave diagram. The wave diagram, along with the state properties, enables one to plot pressure as a function of time. This has been done in figure 20, where calculated and experimental pressure can be compared. The two agree quite well except for some difference in phasing at point B. This is largely because of the critical position of the pressure transducer with respect to the nozzle, as well as the fact that only two area discontinuities have been used in the idealized duct.

Since the analysis of the discharge of compressed air from a duct of variable cross-section proved to be quite accurate, a second wave diagram has been constructed (figure 25), with the following modification: instead of using a pressure vessel of finite size it has been assumed that the pressure vessel contains air that is at all times at the same pressure it would have for operation in the restricted flow direction, but is of infinite cross-section, hence zero velocity. This makes a simple boundary condition, and the assumption of zero velocity in the pressure vessel

makes a negligible difference, since it is quite small in the restricted flow direction. Since the nondimensional speed of sound is used in constructing the wave diagram, the speed of sound, rather than the pressure, is given as a boundary condition in figure 25. The two are related by

$$p = a^7$$

in nondimensional form.

Now the mass flow can be calculated from the known variation in velocity and density at point B. These properties are listed in Table II and the mass lost is plotted as a function of time in figure 23.

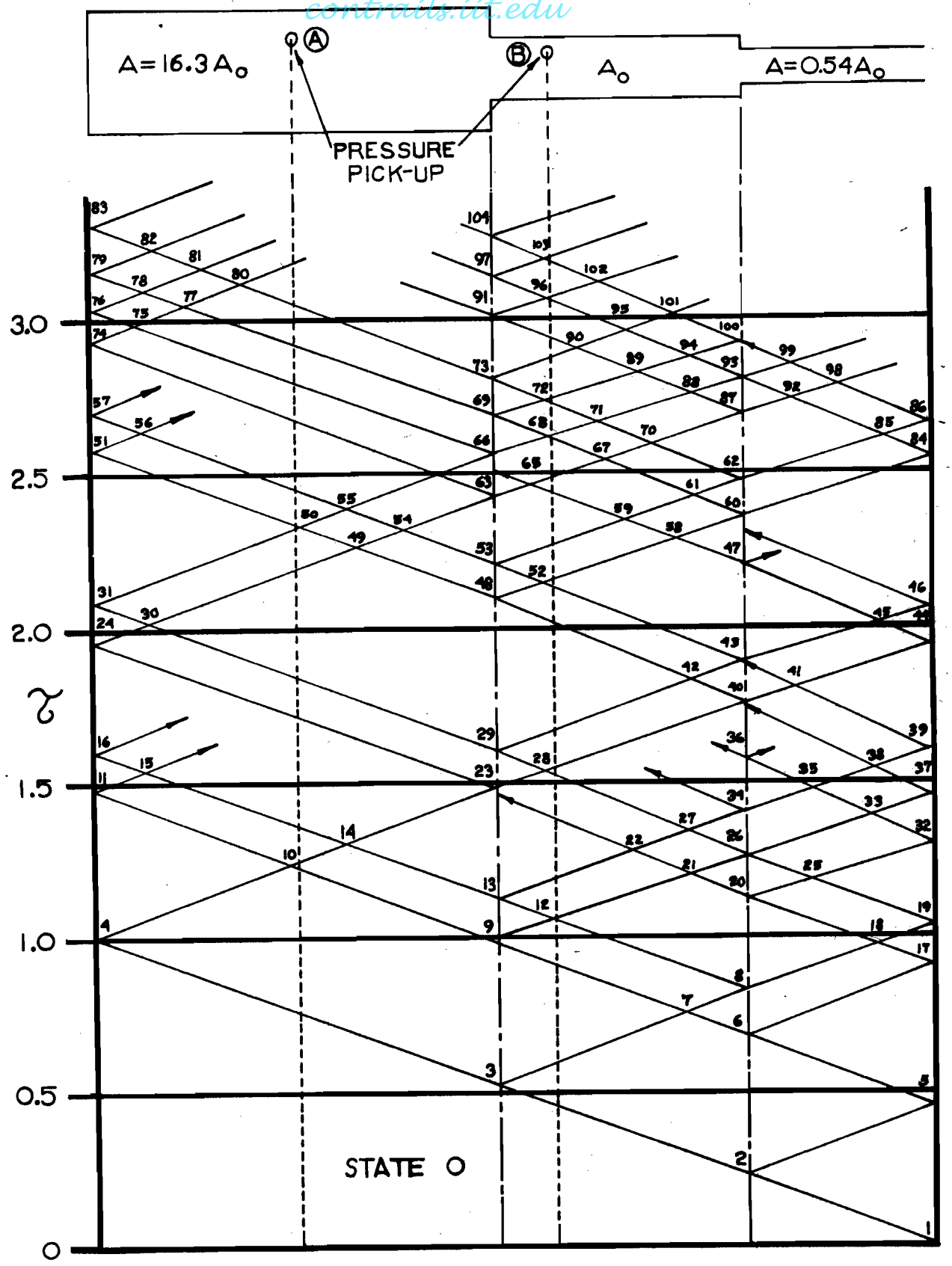

Figure 24. Wave Diagram for Free Flow Discharge.

TABLE II

RIEMANN VARIABLES AND STATE PROPERTIES FOR FREE FLOW DISCHARGE OF COMPRESSED AIR FROM AERODYNAMIC RECTIFIER TEST INSTALLATION*

State	P	Q	u	a	ρ	p (atm.)
0	5.047	5.047	0	1.00945	1.0481	1.0680
1	5.047	4.953	.047	1.0000		
2R	5.074	4.953	.060	1.0028		
2L	5.047	4.984	.032	1.0032	1.0161	1.0232
3R	5.096	4.984	.056	1.0081	1.0411	1.0581
3L	5.047	5.038	.004	1.0084	1.0427	1.0603
4	5.038	5.038	0	1.0076		
5	5.074	4.926	.074	1.0000		
6R	5.079	4.926	.076	1.0006		
6L	5.047	4.963	.042	1.0010		
7	5.096	4.963	.066	1.0059	1.0298	1.0420
8R	5.140	4.926	.107	1.0066		
8L	5.096	4.979	.058	1.0074		
9R	5.115	4.963	.076	1.0078		
9L	5.047	5.038	.004	1.0085		
10	5.038	5.038	0	1.0076	1.0386	1.0544
11	5.038	5.038	0	1.0076		
12	5.115	4.979	.068	1.0094	1.0479	1.0677
13R	5.103	4.979	.062	1.0082	1.0417	1.0588
13L	5.047	5.039	.004	1.0086		
14	5.038	5.039	0	1.0077	1.0391	1.0551
15	5.038	5.039	0	1.0077		
16	5.038	5.038	0	1.0076		
17	5.079	4.921	.079	1.0000		
18	5.140	4.921	.110	1.0061		
19	5.140	4.860	.140	1.0000		
20R	5.141	4.921	.110	1.0062		
20L	5.096	4.975	.060	1.0071		
21	5.115	4.975	.070	1.0090		
22	5.103	4.975	.064	1.0078	1.0396	1.0559
23R	5.087	4.975	.054	1.0066		
23L	5.038	5.031	.003	1.0069	1.0350	1.0493
24	5.031	5.031	0	1.0062		
25	5.141	4.860	.140	1.0001		
26R	5.172	4.860	.157	1.0035		
26L	5.115	4.937	.089	1.0052		
27	5.103	4.937	.083	1.0040		
28	5.087	4.937	.075	1.0024	1.0120	1.0169
29R	5.119	4.937	.091	1.0056	1.0283	1.0399
29L	5.038	5.026	.006	1.0064	1.0324	1.0457
30	5.031	5.026	.003	1.0057	1.0288	1.0425
31	5.026	5.026	0	1.0052		
32	5.141	4.859	.141	1.0000		
33	5.172	4.859	.156	1.0031		
34R	5.164	4.860	.152	1.0024		
34L	5.103	4.937	.083	1.0040		
35	5.164	4.859	.153	1.0023		
36R	5.164	4.859	.153	1.0023		
36L	5.103	4.937	.083	1.0040		
37	5.172	4.828	.172	1.0000		
38	5.164	4.828	.168	.9992		
39	5.164	4.836	.164	1.0000		
40R	5.152	4.828	.162	.9980		

*To supplement wave diagram presented in figure 24.

TABLE II (CONTINUED)

State	P	Q	u	a	ρ	p (atm.)
40L	5.087	4.912	.088	1.0000		
41	5.152	4.836	.158	.9988		
42	5.119	4.912	.103	1.0031	1.0155	1.0219
43R	5.188	4.836	.176	1.0024		
43L	5.119	4.927	.096	1.0046		
44	5.152	4.848	.152	1.0000		
45	5.188	4.848	.170	1.0036		
46	5.188	4.812	.188	1.0000		
47R	5.187	4.848	.170	1.0035		
47L	5.119	4.937	.091	1.0056		
48R	5.136	4.912	.112	1.0049		
48L	5.038	5.024	.007	1.0061		
49	5.031	5.024	.006	1.0055		
50	5.026	5.024	.001	1.0050	1.0252	1.0355
51	5.024	5.024	0	1.0048		
52	5.136	4.927	.105	1.0063	1.0318	1.0449
53R	5.126	4.927	.100	1.0053	1.0267	1.0377
53L	5.038	5.025	.006	1.0063		
54	5.031	5.025	.003	1.0056		
55	5.026	5.025	.001	1.0051	1.0257	1.0362
59	5.126	4.937	.095	1.0063	1.0318	1.0449
60R	5.212	4.812	.200	1.0025		
60L	5.136	4.917	.109	1.0053		
62R	5.193	4.812	.191	1.0007		
62L	5.126	4.905	.110	1.0031		
63R	5.114	4.927	.094	1.0041		
63L	5.031	5.019	.006	1.0050		
65	5.114	4.937	.088	1.0051	1.0257	1.0363
66R	5.095	4.937	.079	1.0033		
66L	5.025	5.015	.005	1.0040	1.0201	1.0283
67	5.114	4.917	.098	1.0031		
68	5.095	4.917	.089	1.0012	1.0060	1.0084
69R	5.109	4.917	.096	1.0026		
69L	5.025	5.013	.006	1.0038	1.0191	1.0268
71	5.095	4.905	.095	1.0000		
72	5.109	4.905	.100	1.0014	1.0070	1.0098
73R	5.120	4.905	.108	1.0025	1.0125	1.0176
73L	5.025	5.011	.007	1.0037	1.0186	1.0261
84	5.212	4.788	.212	1.0000		
86	5.193	4.807	.193	1.0000		
87R	5.188	4.812	.188	1.0000		
87L	5.114	4.910	.102	1.0025		
88	5.095	4.910	.092	1.0005		
90	5.120	4.910	.105	1.0030	1.0150	1.0212
91R	5.115	4.910	.102	1.0025		
91L	5.025	5.012	.006	1.0037		
92	5.188	4.788	.200	.9976		
93R	5.172	4.788	.192	.9959		
93L	5.095	4.889	.103	.9985		
94	5.109	4.889	.110	.9998		
95	5.120	4.889	.115	1.0009		
96	5.115	4.889	.113	1.0004	1.0020	1.0028
97R	5.131	4.889	.121	1.0020		
97L	5.025	5.009	.008	1.0035		
99	5.172	4.807	.182	.9979		
100R	5.181	4.807	.187	.9988		
100L	5.109	4.905	.102	1.0013		
102	5.115	4.905	.105	1.0020		
103	5.131	4.905	.113	1.0036	1.0181	1.0255

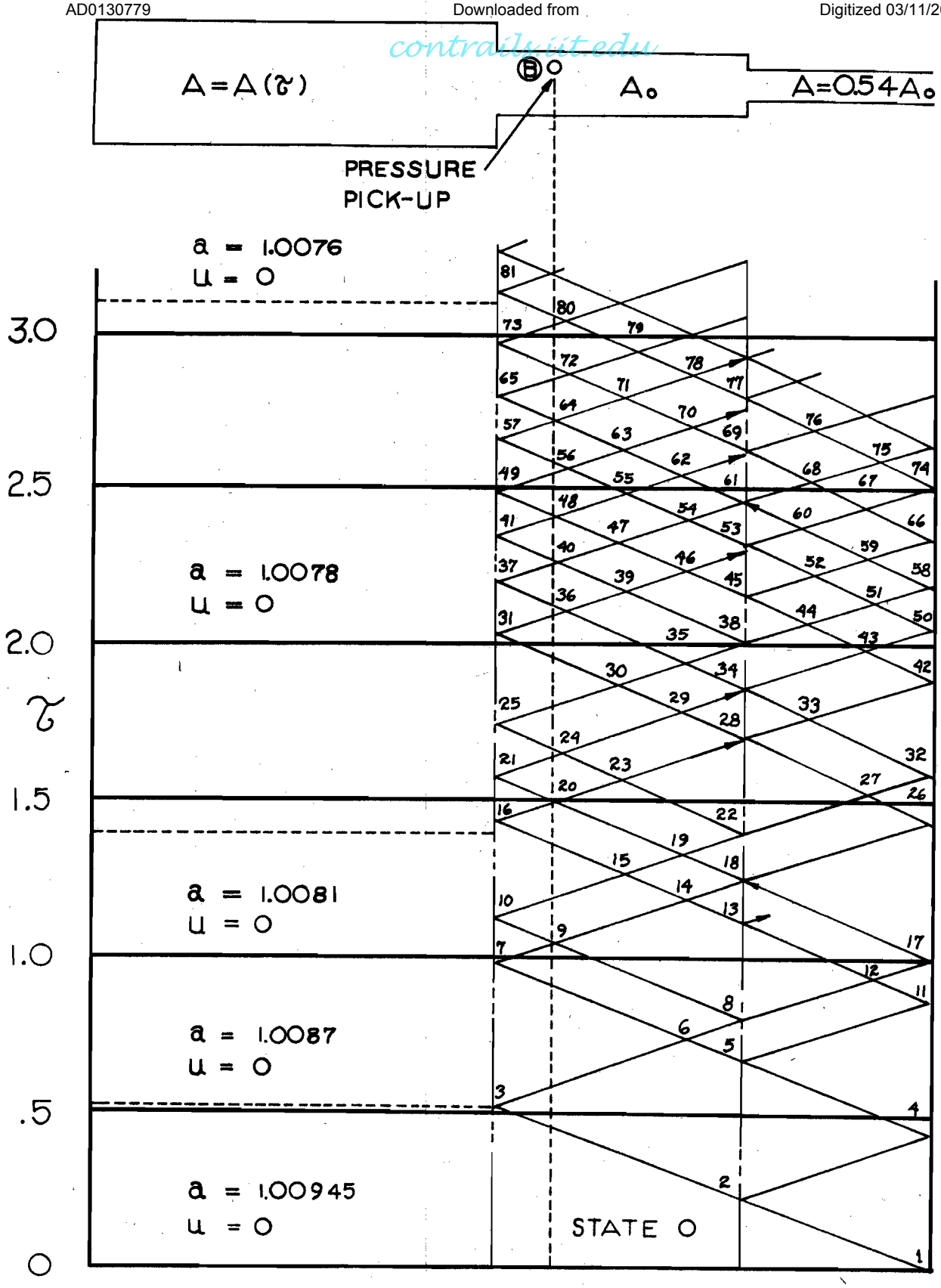

Figure 25. Wave Diagram for Modified Free Flow Discharge.

TABLE III

RIEMANN VARIABLES AND STATE PROPERTIES FOR MODIFIED FREE FLOW DISCHARGE OF COMPRESSED AIR THROUGH AERODYNAMIC RECTIFIER*

State	P	Q	u	a	ρ	p (atm.)
0	5.047	5.047	0	1.00945	1.0481	1.0680
1	5.047	4.953	.047	1.0000		
2R	5.074	4.953	.060	1.0028		
2L	5.047	4.989	.032	1.0032	1.0161	1.0232
3	5.096	4.984	.056	1.0081	1.0411	1.0581
4	5.074	4.926	.074	1.0000		
5R	5.080	4.926	.077	1.0006		
5L	5.047	4.963	.042	1.0010		
6	5.096	4.963	.066	1.0059	1.0298	1.0420
7	5.117	4.963	.077	1.0081		
8R	5.142	4.926	.108	1.0068		
8L	5.096	4.980	.058	1.0076		
9	5.117	4.980	.068	1.0097	1.0494	1.0698
10	5.096	4.980	.058	1.0077	1.0390	1.0551
11	5.080	4.920	.080	1.0000		
12	5.142	4.920	.111	1.0062		
13R	5.142	4.920	.111	1.0062		
13L	5.096	4.974	.061	1.0070		
14	5.117	4.974	.072	1.0091		
15	5.096	4.974	.061	1.0070	1.0354	1.0500
16	5.100	4.974	.063	1.0074		
17	5.142	4.858	.142	1.0000		
18R	5.180	4.858	.161	1.0039		
18L	5.117	4.940	.088	1.0057		
19	5.096	4.940	.078	1.0036		
20	5.100	4.940	.080	1.0040	1.0201	1.0283
21	5.128	4.940	.094	1.0069	1.0349	1.0493
22R	5.155	4.858	.149	1.0013		
22L	5.096	4.932	.082	1.0028		
23	5.100	4.932	.084	1.0032		
24	5.128	4.932	.098	1.0060	1.0303	1.0427
25	5.136	4.932	.102	1.0067	1.0339	1.0478
26	5.180	4.820	.180	1.0000		
27	5.155	4.820	.168	.9975		
28R	5.168	4.820	.174	.9989		
28L	5.100	4.911	.095	1.0011		
29	5.128	4.911	.108	1.0039		
30	5.136	4.911	.112	1.0047	1.0237	1.0333
31	5.155	4.911	.120	1.0063	1.0318	1.0449
32	5.155	4.845	.155	1.0000		
33	5.168	4.845	.162	1.0013		
34R	5.196	4.845	.170	1.0052		
34L	5.128	4.943	.093	1.0072		
35	5.136	4.943	.096	1.0079		
36	5.155	4.943	.106	1.0098	1.0499	1.0706
37	5.126	4.943	.092	1.0069		
38R	5.207	4.845	.181	1.0053		
38L	5.136	4.939	.098	1.0075		
39	5.155	4.939	.108	1.0094		
40	5.126	4.939	.094	1.0065	1.0329	1.0463
41	5.129	4.939	.095	1.0068	1.0344	1.0485
42	5.168	4.832	.168	1.0000		
43	5.196	4.832	.182	1.0028		

*To supplement wave diagram presented in figure 25.

TABLE III (CONTINUED)

State	P	Q	u	a	ρ	p (atm.)
44	5.207	4.832	.188	1.0039		
45R	5.209	4.832	.189	1.0041		
45L	5.136	4.931	.102	1.0066		
46	5.155	4.931	.112	1.0086		
47	5.126	4.931	.092	1.0057		
48	5.129	4.931	.094	1.0060	1.0303	1.0427
49	5.135	4.931	.102	1.0067	1.0339	1.0478
50	5.196	4.804	.196	1.0000		
51	5.207	4.804	.202	1.0011		
52	5.209	4.804	.202	1.0013		
53R	5.236	4.804	.216	1.0041		
53L	5.155	4.919	.118	1.0074		
54	5.126	4.919	.104	1.0045		
55	5.129	4.919	.105	1.0048		
56	5.135	4.919	.108	1.0054	1.0272	1.0384
57	5.146	4.919	.114	1.0065		
58	5.207	4.793	.207	1.0000		
59	5.209	4.793	.208	1.0002		
60	5.236	4.793	.222	1.0029		
61R	5.205	4.793	.206	.9998		
61L	5.126	4.902	.112	1.0027		
62	5.129	4.902	.114	1.0031		
63	5.135	4.902	.116	1.0037		
64	5.146	4.902	.122	1.0048	1.0242	1.0340
65	5.135	4.902	.129	1.0061	1.0308	1.0434
66	5.209	4.791	.209	1.0000		
67	5.236	4.791	.222	1.0027		
68	5.205	4.791	.207	.9996		
69R	5.207	4.791	.208	.9999		
69L	5.129	4.901	.114	1.0029		
70	5.135	4.901	.117	1.0036		
71	5.146	4.901	.122	1.0047		
72	5.135	4.901	.117	1.0036	1.0181	1.0254
73	5.160	4.901	.129	1.0061	1.0308	1.0434
74	5.236	4.764	.236	1.0000		
75	5.205	4.764	.220	.9969		
76	5.207	4.764	.221	.9971		
77R	5.220	4.764	.228	.9985		
77L	5.135	4.886	.124	1.0021		
78	5.146	4.886	.130	1.0032		
79	5.135	4.886	.124	1.0021		
80	5.160	4.886	.137	1.0046	1.0232	1.0326
81	5.169	4.886	.141	1.0056		

APPENDIX II

ANALYSIS OF SHOCK TUBE TEST RESULTS

A typical result from a shock tube test is shown in figure 26. The time scale is 2 milliseconds per centimeter, or division, so that the total width of the grid is 20 milliseconds. Furthermore, because of the photographic processes involved in recording oscilloscope traces with a polaroid camera, time is measured from right to left.

Consider first the trace which starts in the lower right hand corner. This trace has a vertical pressure scale of 0.476 psi per centimeter. One millisecond after the arrival of the shock wave at the first pressure transducer, which was used to start the sweep, the pressure at the second pressure transducer jumps to 0.95 psi. The time of one millisecond is the time for the shock wave to reach the second transducer and is in agreement with the actual distance of one foot between the first and second transducers. After two milliseconds the pressure takes another jump, this time to about 1.95 psi. The timing is just right to correspond to the reflection of a compression wave from the bullet-like nose of the aerodynamic rectifier. However, the magnitute of the pressure rise, which indicates total reflection, has not been understandable. Hence no attempt has been made to get quantatative data from these tests in regards to mass flow. At any rate, the pressure upstream from the rectifier holds fairly constant at about 1.8 psi if the ringing is smoothed out.

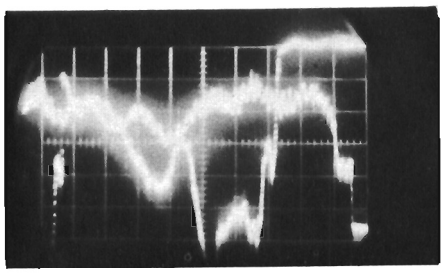

Figure 26
Shock Tube Trace

Now consider the trace which starts in the upper right hand corner. The vertical scale is inverted and of magnitude 0.24 psi per centimeter. Nothing happens for a little over five milliseconds. At that time the transmitted shock wave arrives and the pressure rises to a maximum of about 1.40 psi. Ten milliseconds after the sweep has been triggered, the pressure starts falling to the steady state condition. Steady state has been nearly achieved sixteen milliseconds after the sweep has been triggered. This corresponds to a time of about fourteen milliseconds after the arrival of the initial shock wave at the first few turning blades. The sudden rise in pressure after nineteen milliseconds is from the shock wave reflected from the closed end of the shock tube.